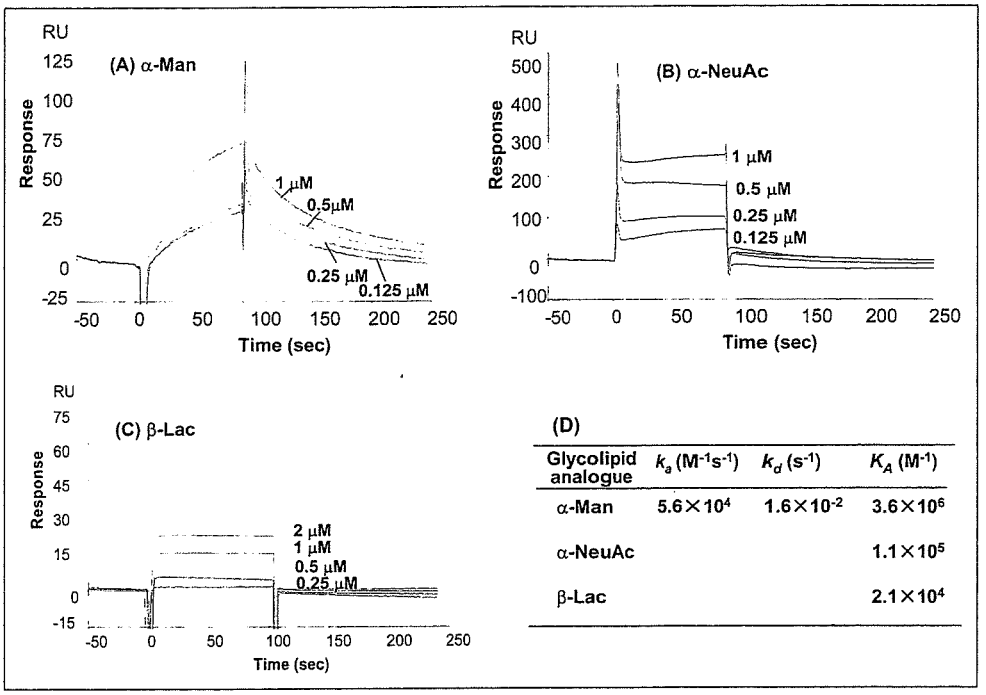

(D)

Glycolipid analogue	k_a ($M^{-1}s^{-1}$)	k_d (s^{-1})	K_A (M^{-1})
α-Man	5.6×10^4	1.6×10^{-2}	3.6×10^6
α-NeuAc			1.1×10^5
β-Lac			2.1×10^4

FIGURE 2. **Quantification of interaction between PPT and glycolipid analogues by SPR.** Glycolipid analogues were immobilized on an HPA sensor chip as described in the text. PPT was pretreated with 0.1 mM PMSF and injected onto the sensor chip at various concentrations in 10 mM TBS buffer (pH 7.5) at a flow rate of 20 μl/min at 25 °C using BIAcore. Binding curves of PPT on the sensor chip immobilized with glycolipid analogues containing α-Man (*A*), α-NeuAc (*B*), and β-Lac (*C*) are shown. The response is expressed as the change in the number of resonance units induced by the binding of PPT to the glycolipid analogue-immobilized flow cell, which was corrected for bulk effect by subtracting the change on the phosphatidylcholine-immobilized reference cell. *D*, kinetic parameters for the interaction between PPT and glycolipid analogues. Kinetic parameters were calculated by global analysis for α-Man and affinity analysis for α-NeuAc and β-Lac. k_a, association rate constant; k_d, dissociation rate constant; K_A, association constant.

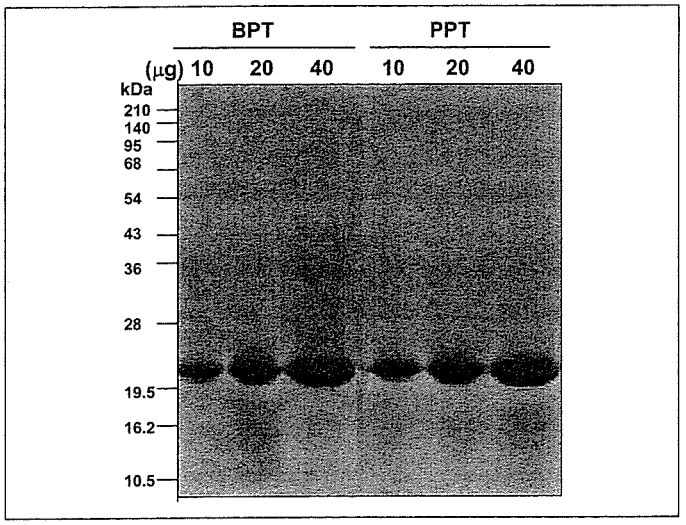

FIGURE 3. **SDS-PAGE of BPT and PPT.** Bovine and porcine trypsin (10, 20, or 40 μg of protein per lane) were loaded under reduced condition onto a 14% polyacrylamide gel. SDS-PAGE was performed as described in the text, and protein bands were visualized by Coomassie Brilliant Blue R-250. The migration positions of molecular weight markers are shown on the *left side* of the gel.

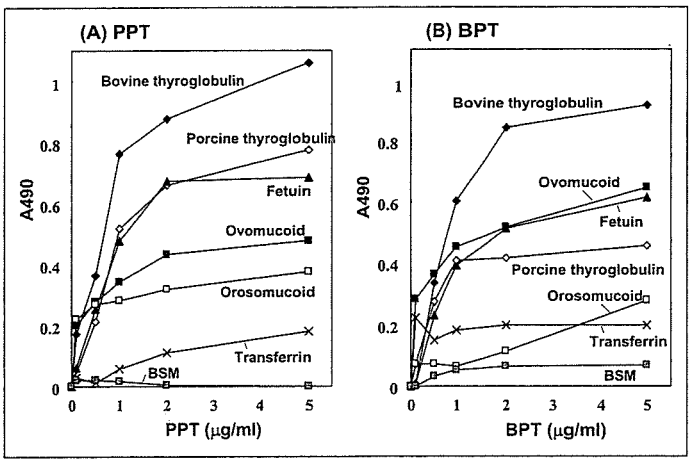

FIGURE 4. **Reactivities of PPT (*A*) and BPT (*B*) to biotinylated glycoproteins by ELISA.** PPT or BPT (each 100 μl) was coated onto the wells of a microtiter plate and reacted with various glycoprotein probes as described in the text. The bound glycoprotein probes were detected with ABC complex and o-phenylenediamine/H_2O_2 by ELISA. Symbols used are: ◆, bovine thyroglobulin; ◇, porcine thyroglobulin; ▲, fetuin; ■, ovomucoid; □, orosomucoid; ×, transferrin; and ▨, BSM.

mM TBS (pH 7.5) were separately injected onto the trypsin-immobilized sensor chip at concentrations of 1, 0.5, 0.25, 0.125, and 0.0625 μM for 150 s at a flow rate of 20 μl/min at 25 °C. The chip was regenerated each time by injection of 20 μl of 10 mM HCl. To assay inhibition, a trypsin-immobilized sensor chip was equilibrated with TBS containing 50 mM or 0.2 M methyl-α-mannoside, methyl-α-galactoside, or lactose for 15 min, and then the glycoprotein dissolved in the same buffer was injected. Kinetic parameters were calculated mainly by global analysis, or affinity analysis when necessary, using the BIAevaluation software version 3.1.

Measurement of Enzyme Activity of Trypsin—Enzyme activity was measured in a test tube according to the method previously described using BAEE (11) or BAPA (12) as the substrate. To estimate the effect of sugar on the BAEE-hydrolytic activity, it was measured after preincubation of PPT in 100 μl of 1 mM HCl (0.02 mg/ml) with 100 μl of 0.2 M methyl-α-D-mannoside, 0.2 M methyl-α-D-galactoside, or 0.2 M lactose in 20 mM TBS (pH 7.6) for 10 min at 25 °C. A control experiment was done by preincubating PPT without sugar. After preincubation, the PPT solution was added to 500 μl of 0.025 mM BAEE in 10 mM TBS (pH 7.6) and incubated at 25 °C for 1 min. Absorbance was immediately measured at 253 nm, and trypsin activity that increased absorbance by 0.003 at 25 °C for 1 min was regarded as 1 USP unit of trypsin.

To analyze the effect of sugar by a double reciprocal Lineweaver-Burk plot, the initial rates of the enzyme-catalyzed reaction were measured using BAPA as the substrate. The substrate stock solution was prepared by dissolving 0.0217 g of BAPA in 1.5 ml of Me_2SO and then diluted to final concentrations of 0.1–0.5 mM with 100 mM TBS (pH 7.5) in the presence or absence of 0.2 M methyl-α-mannoside, methyl-α-galacto-

side, or lactose. The substrate solutions were heated for 5 min at 37 °C. The enzyme stock solution was prepared by dissolving 2.5 mg of PPT in 3 ml of 1 mM HCl containing 13 mg of $CaCl_2$-$2H_2O$. A 10-μl aliquot of the enzyme solution was added to 3 ml of the substrate solution, and absorbance was measured at 410 nm every 30 s.

RESULTS

Interaction between Trypsins and Sugar-BP Probes

The carbohydrate-binding activities of BPT and PPT were analyzed using synthetic sugar-BP probes (Scheme 2*A*), and specificities toward sugar residues and oligosaccharides were determined. As shown in Fig. 1, both BPT and PPT exhibited high binding activity toward α-Man-, α-Man-6-phosphate-, NeuAcα2,6Galβ1,4Glc-, α-Gal-, and β-Glc-BP probes among the 17 kinds of sugar-BP probes tested. Both trypsins bound to NeuAcα2,3Galβ1,4Glc- and NeuAc-BP to a lesser extent than to NeuAcα2,6Galβ1,4Glc-BP, indicating a preference for sialyl linkages. On the contrary, trypsin did not bind with α-GalNAc- or mucin core 2-type BP probes or with β-Gal, LacNAc, Lac, β-GlcNAc, or β-Gal3-sulfate-BP probes. None of the carbohydrate-binding activities of the trypsins was affected by preincubation with PMSF and EDTA or soybean trypsin inhibitor, suggesting that binding is independent of the catalytic site. The bound sugar residues other than β-D-Glc are components of *N*-glycans, demonstrating basic specificities toward monosaccharides or short sequences that include linkages for trypsin binding.

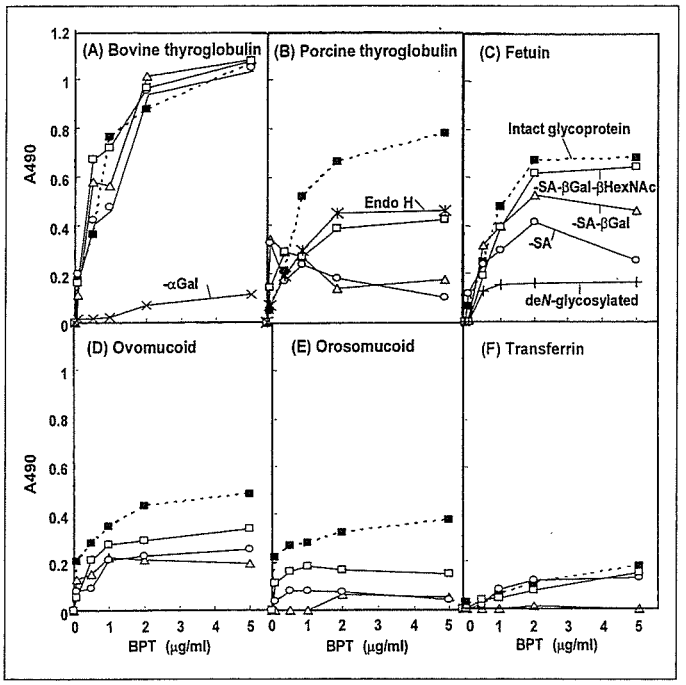

FIGURE 5. **Reactivities of BPT to biotinylated glycoprotein probes before and after glycosidase treatment by ELISA.** Biotinylated glycoprotein probes were pretreated with various exoglycosidases as described in the text. BPT (100 μl) was coated onto the wells of a microtiter plate and reacted with biotinylated glycoprotein probes: bovine thyroglobulin (*A*), porcine thyroglobulin (*B*), fetuin (*C*), ovomucoid (*D*), orosomucoid (*E*), and transferrin (*F*). The bound glycoprotein probes were detected by ELISA as described in the text. Symbols used are: ■, intact; ○, asialo-treated; △, asialoagalacto-treated; □, asialoagalactoahexosamino-treated; ×, α-galactosidase-treated; letter "x" with a vertical line, endoglycosidase H-treated; and +, de-*N*-glycosylated glycoproteins.

Interaction between Trypsin and Glycolipid Analogues Analyzed by SPR

To verify the carbohydrate-binding specificity of trypsin by quantitative measurement, interaction analyses were performed by SPR using five kinds of synthetic high sensitivity glycolipid analogues (Scheme 2*B*). The total amounts of immobilized glycolipid analogues containing α-Man, α-NeuAc, and β-Lac were 1593, 1560, and 1680 BIAcore resonance units (RU, 1000 RU = 1 ng/mm^2), respectively. As shown in Fig. 2 (*A–C*), PPT concentration-dependently bound to immobilized glycolipid analogues. The differential binding of PPT to the analogues clearly indicates its relative binding affinity toward sugar residues: PPT binds best with the analogues containing α-Man, then α-NeuAc, and to a lesser extent β-Lac. The binding and dissociation occurred rapidly at the start and end of injection of the glycolipid analogues except the α-Man derivative, demonstrating the specific binding of PPT to those glycolipid analogues with quick association and dissociation rates. PPT did not bind to other analogues containing β-galactose or β-GlcNAc even at 2 μM. The association constants (K_A) were calculated to be 10^6-10^5 (M^{-1}) for glycolipid analogues containing α-Man and α-NeuAc (Fig. 2*D*), which are comparable to the K_A obtained for the interaction between ricin and the glycolipid analogues containing β-galactose[3] and higher than that obtained between concanavalin A and α-Man-derivatized glycolipid containing phosphatidylethanolamine aglycon (13). The carbohydrate-binding specificity indicated by SPR corresponded with that obtained by using sugar-BP probes (Fig. 1) demonstrating that the affinity of trypsin for specific carbohydrates is comparable to those of known plant lectins. Therefore, the binding activity of trypsin for glycoproteins was examined.

Purity of BPT and PPT on SDS-PAGE

The carbohydrate-binding activities shown in Figs. 1 and 2 have never been reported for trypsin. To eliminate the suspicion that some contaminant in the trypsin preparation might exhibit such an activity, we analyzed the purity of the trypsin preparations used in this study by SDS-PAGE. As shown in Fig. 3, both BPT and PPT showed only a single band without any detectable contamination even if 40 μg of trypsin preparation was applied per lane to the polyacrylamide gel. Therefore, the carbohydrate-binding activities observed in this study were attributed to the trypsins.

[3] H. Takekawa, C. Ina, R. Sato, K. Toma, and H. Ogawa, unpublished results.

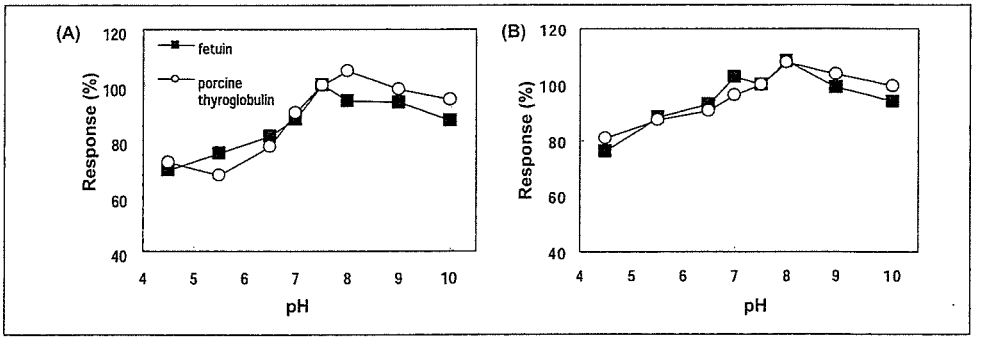

FIGURE 6. **Binding of trypsin to fetuin and porcine thyroglobulin at various pH by SPR.** PPT and BPT were immobilized on a CM5 sensor chip, and each glycoprotein was injected onto the sensor chip at various pH, as described in the text. Fetuin (■) or porcine thyroglobulin (○) was dissolved at concentrations of 1 or 0.5 μM, respectively, in 10 mM acetate buffer (pH 4.5–6.5), 10 mM TBS (pH 7–8), or 10 mM bicarbonate buffer (pH 9–10) and injected onto the sensor chip. The bound amounts of glycoprotein are expressed as relative response (%) by taking the response at pH 7.5 as 100%. *A*, relative response on immobilized PPT; *B*, relative response on immobilized BPT.

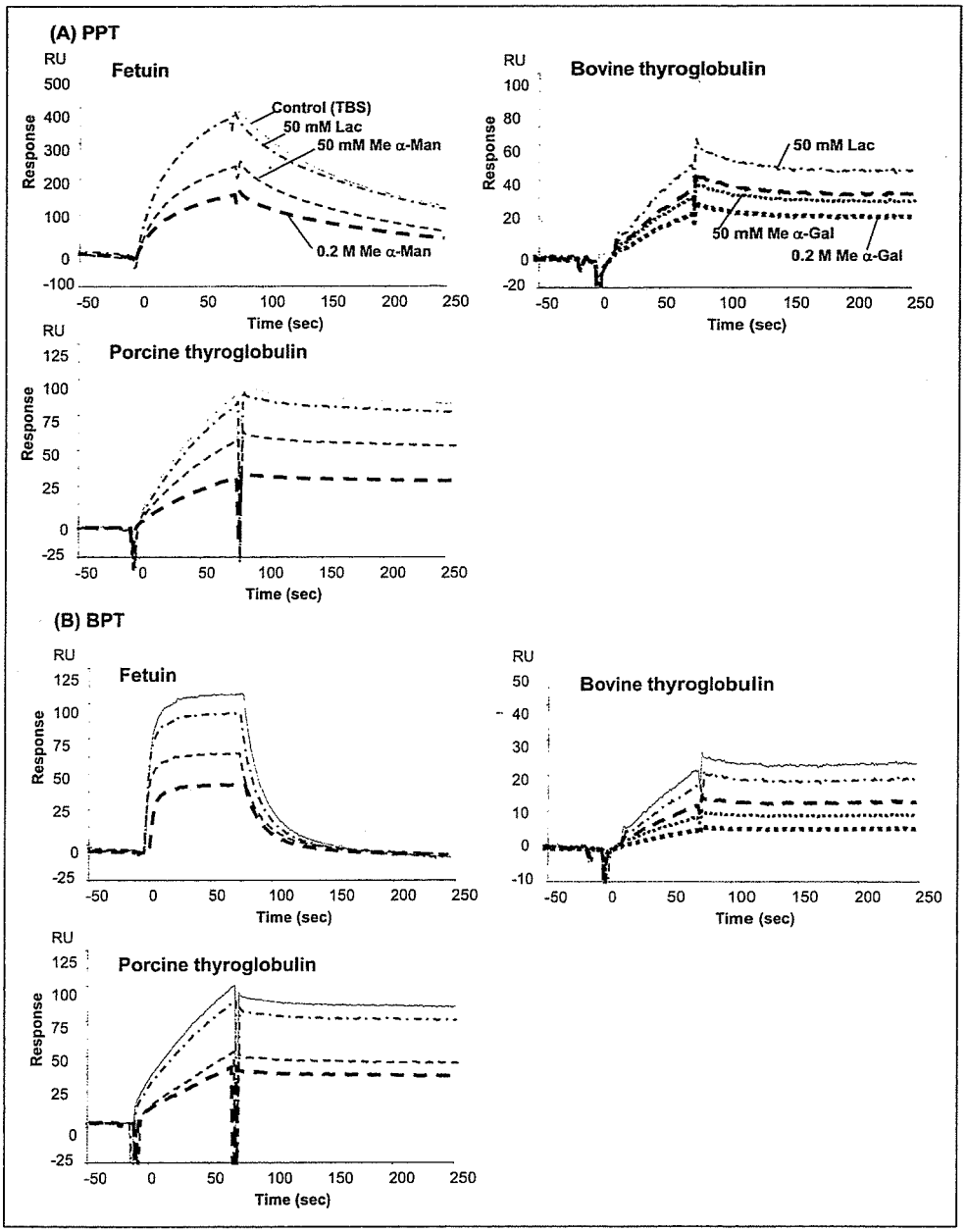

FIGURE 7. **Effect of sugars on interaction between trypsins and glycoproteins.** Trypsins were immobilized on the sensor chip and preincubated with 50 mM or 0.2 M methyl-α-D-mannoside, lactose, or methyl-α-D-galactoside, and then the glycoprotein solution in 10 mM TBS (pH 7.5) or TBS containing each sugar at a concentration of 50 mM or 0.2 M was injected onto the immobilized trypsins. *A*, the binding curves of glycoproteins to PPT, and *B*, the binding curves of glycoproteins to BPT. *Solid line*, control without sugar; *light dashed line*, 50 mM methyl-α-D-mannoside; *heavy dashed line*, 0.2 M methyl-α-D-mannoside; *light dotted line*, 50 mM methyl-α-D-galactoside; *heavy dotted line*, 0.2 M methyl-α-D-galactoside; and *dashed* and *dotted line*, 50 mM Lac.

Interaction between Trypsins and Biotinylated Glycoprotein Probes

Interactions between the glycoprotein probes and PPT or BPT were studied by ELISA at pH 7.5, which is the physiological pH in the duodenum. Because the amount of biotin incorporated into each glycoprotein probe was almost equal, as judged by the color intensity of each probe developed with the ABC complex being within a 10% error, the value of A_{490} corresponds to the amount of probe bound. As shown in Fig. 4(*A* and *B*), BPT and PPT were found to bind to various glycoproteins with very similar binding patterns. The trypsins bound best to bovine thyroglobulin and to a lesser extent to fetuin, porcine thyroglobulin, ovomucoid, orosomucoid, and transferrin, in that order, but not to BSM. All the bound glycoproteins contain 5–30% (w/w) *N*-linked oligosaccharides, whereas BSM possesses up to 60% (w/w) *O*-linked glycans, which are mainly sialyl-Tn and core 3-type (Scheme 1). Combined with the finding that trypsins did not bind with α-GalNAc- and β-GlcNAc (Fig. 1), this indicates that trypsins do not interact with *O*-linked glycans.

The involvement of the *N*-glycan structure in the binding with PPT and BPT was shown by deglycosylating the glycoprotein probes with endo-type glycosidases. As shown in Fig. 5*C*, de-*N*-glycosylation of fetuin by *N*-glycosidase F treatment markedly decreased the reactivity toward both trypsins (data not shown for PPT), showing that their binding was mostly due to the affinity for the sialylated complex-type *N*-glycans of fetuin. The reactivity of trypsins for porcine thyroglobulin (Fig. 5*B*), which contains almost equal amounts of high Man-type and complex-type glycans (Scheme 1), was decreased to about half that of intact porcine thyroglobulin by endoglycosidase H treatment as well as asialoagalactoahexosaminylation, indicating that trypsins bind with high Man-type *N*-glycans as well as the sialylated complex-type.

As shown in Fig. 5, the effects of exo-type glycosidase treatments of the glycoprotein probes illustrate the contribution of each sugar residue to the interaction with BPT. Remarkably, binding of BPT with bovine thyroglobulin was found to be diminished by α-galactosidase treatment (Fig. 5*A*), clearly indicating that the α-galactosyl residue at the nonreducing terminal, which is unique to the *N*-glycan of bovine thyroglobulin (Scheme 1), is an epitope for BPT binding. Other exoglycosidase treatments of bovine thyroglobulin did not affect the binding.

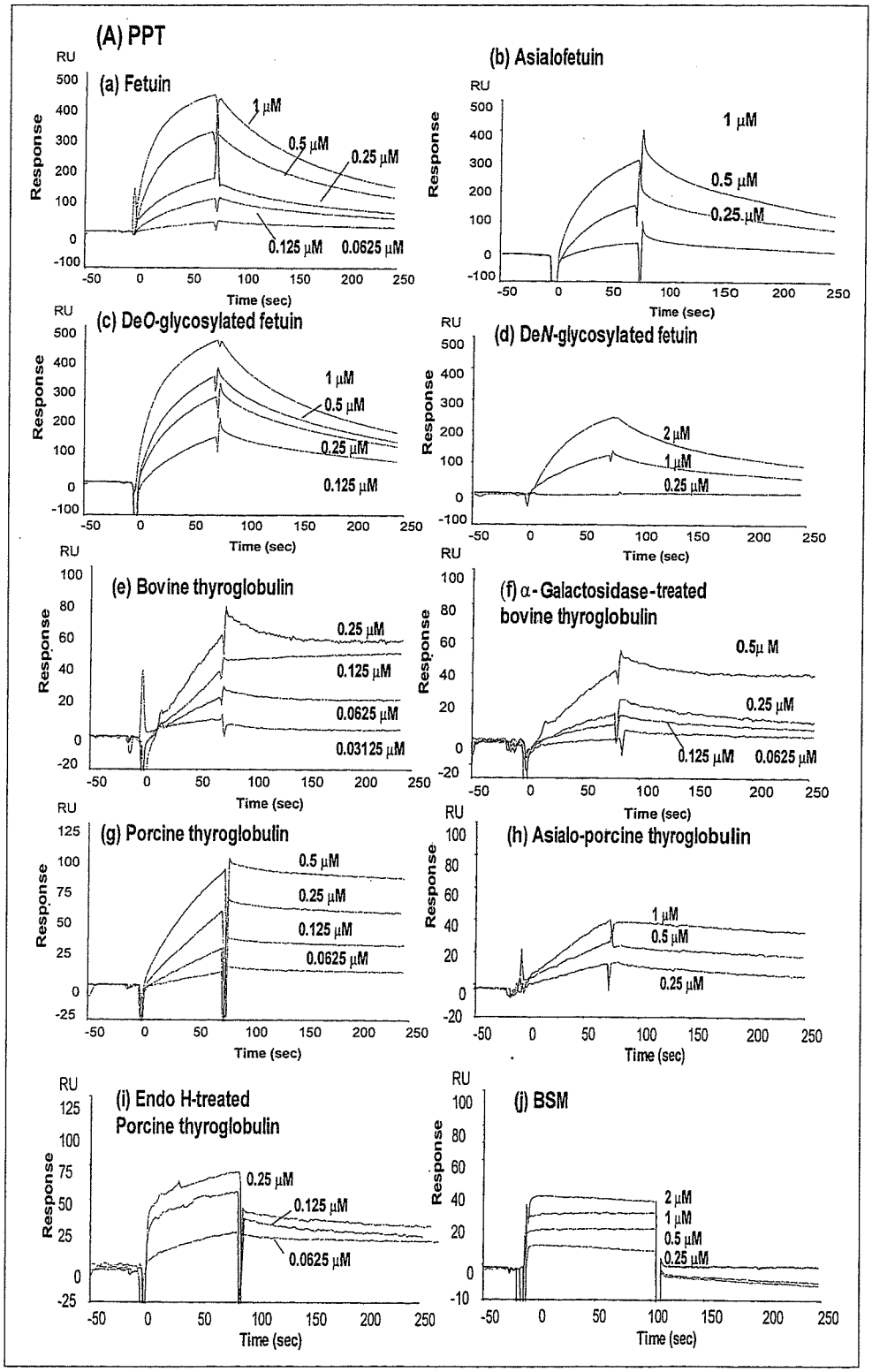

FIGURE 8. **Quantification of interaction between trypsins and glycoproteins by SPR.** PPT and BPT were immobilized on a CM5 sensor chip as described in the text. Glycoproteins were injected onto a trypsin-immobilized sensor chip in 10 mM TBS (pH 7.5) for 150 s at a flow rate of 20 ml/min at 25 °C. The response was expressed as the change of resonance units induced by the binding of fetuin to the trypsin-immobilized flow cell, which was corrected for bulk effect by subtracting the change on the BSA-immobilized reference cell. Binding curves of glycoproteins on the sensor chip were immobilized with PPT (*A*) and BPT (*B*).

On the other hand, neuraminidase treatment of other glycoproteins that possess sialylated complex-type *N*-glycans, such as fetuin, ovomucoid, orosomucoid, and porcine thyroglobulin, considerably decreased the binding, as shown in Fig. 5 (*B–E*). For these glycoprotein probes β-galactosidase treatment subsequent to desialylation did not significantly change the binding, but exposure of α-mannosyl residues of the trimannosyl core of *N*-glycans by β-hexosaminidase treatment subsequent to degalactosylation restored the binding to trypsin. These results strongly indicate that α-NeuAc and α-mannosyl residues of complex-type multiantennary *N*-glycans contribute to the binding of trypsins, but β-galactose and β-GlcNAc residues of the lactosamine sequence do not. The biantennary complex type of transferrin did not show significant affinity for trypsins (Fig. 5*F*). As a whole, the sugar-binding specificities of BPT and PPT indicated in Fig. 1 coincide with and account for the binding specificities toward the glycoprotein probes.

Preincubation of PPT and BPT with PMSF and EDTA or soybean

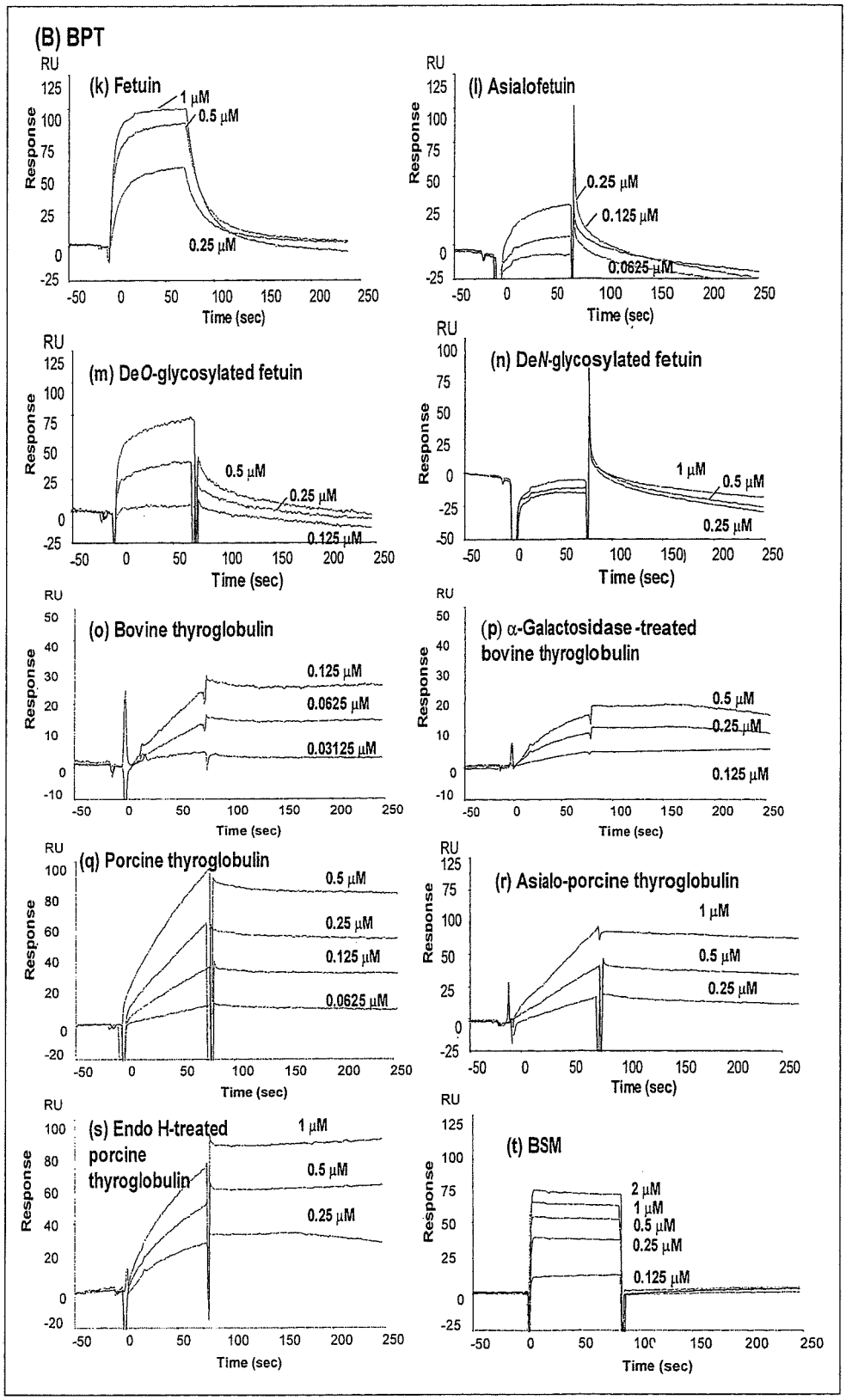

FIGURE 8—*continued*

trypsin inhibitor before the binding studies did not affect the binding activities toward glycoproteins (data not shown). Moreover, the binding of trypsin to ovomucoid, a natural inhibitor that blocks the catalytic site of trypsin, was found to be significantly affected by glycan trimming (Fig. 5*D*). The observations indicate that the trypsin binding to glycoproteins is independent of their catalytic activity.

Interaction between Trypsins and Various Glycoproteins Analyzed by BIAcore

The total amounts of immobilized PPT, BPT, and BSA were 4,012, 4,028, and 4,031 RU, respectively. The responses are expressed as the change of resonance units induced by the binding of analytes to each

TABLE 1

Binding parameters for interaction between trypsins and glycoproteins

Interactions between trypsin and glycoproteins were measured in 10 mM TBS (pH 7.5) using BIAcore. Kinetics parameters were calculated by global analysis for most glycoproteins and affinity analysis for BSM. k_a, association rate constant; k_d, dissociation rate constant; K_A, association constant ($K_A = k_a/k_a$).

	k_a	k_d	K_A
	$M^{-1}\,s^{-1}$	s^{-1}	M^{-1}
(A) PPT			
Bovine thyroglobulin	3.97×10^3	2.47×10^{-7}	1.61×10^{10}
α-Galactosidase-treated bovine thyroglobulin	7.23×10	5.67×10^{-5}	1.28×10^5
Porcine thyroglobulin	3.05×10^4	7.27×10^{-4}	4.19×10^7
Asialo-porcine thyroglobulin	8.52×10^3	1.35×10^{-3}	6.30×10^6
Endo H-treated thyroglobulin	1.04×10^4	1.36×10^{-3}	7.68×10^6
Fetuin	5.07×10^4	6.20×10^{-3}	8.17×10^6
Asialo-fetuin	1.26×10^4	6.04×10^{-3}	2.09×10^6
De-*O*-glycosylated fetuin	4.57×10^4	5.46×10^{-3}	8.38×10^6
De-*N*-glycosylated fetuin	9.71×10	4.67×10^{-3}	2.08×10^4
BSM			1.08×10^4
(B) BPT			
Bovine thyroglobulin	1.55×10^4	1.45×10^{-6}	1.07×10^{10}
α-Galactosidase-treated bovine thyroglobulin	3.19×10	9.07×10^{-5}	3.51×10^5
Porcine thyroglobulin	3.06×10^4	6.38×10^{-4}	4.79×10^7
Asialo-porcine thyroglobulin	4.28×10^3	6.08×10^{-4}	7.04×10^6
Endo H-treated thyroglobulin	3.49×10^2	5.33×10^{-5}	6.55×10^6
Fetuin	2.43×10^4	5.67×10^{-3}	4.30×10^6
Asialo-fetuin	9.13×10^3	7.13×10^{-3}	1.28×10^6
De-*O*-glycosylated fetuin	1.79×10^4	5.40×10^{-3}	3.32×10^6
De-*N*-glycosylated fetuin	1.09×10^2	1.86×10^{-2}	5.87×10^3
BSM			8.09×10^4

flow cell, which was corrected for bulk effect by subtracting the change on the BSA-immobilized reference cell.

pH Dependence of Interaction between Trypsin and Glycoproteins—Fetuin or porcine thyroglobulin was injected onto a trypsin-immobilized chip at pH 4.5–10. As shown in Fig. 6, the amounts of the glycoproteins bound to immobilized PPT and BPT changed within 30% in the pH range examined, showing a maximum at around pH 7.5–8.0. The weakly alkaline pH coincides with the enteric pH indicating that the carbohydrate-binding activity of trypsin is optimal in the milieu of the intestine. Based on this observation, 10 mM TBS at pH 7.5 was thereafter used for the binding studies.

Effect of Sugars on Binding of Trypsin to Glycoproteins—Fig. 7 shows the effect of monosaccharide trypsin binding to glycoproteins. Me-α-Man and Me-α-galactoside, which showed the highest binding to trypsin (Fig. 1) were used as inhibitors in comparison with Lac, which showed relatively lower binding in the binding study with BP-sugars. The binding of both trypsins to fetuin and porcine thyroglobulins was decreased by 30–44% in 50 mM Me-α-Man and 56–64% in 0.2 M Me-α-Man, and binding to bovine thyroglobulin was decreased by 44–50% and 66–70% in 50 mM and 0.2 M Me-α-Gal, respectively. The binding of trypsins was decreased by only 10–18% even at 0.2 M Lac, indicating the weak inhibitory activity of Lac compared with those of Me-α-Man and Me-α-galactoside coinciding with the relative affinity of sugars shown by BP-sugar binding studies. The results strongly support the hypothesis that trypsins bind glycoproteins by sugar-specific interaction.

Kinetic Parameters for Binding between Trypsins and Glycoproteins—The sensorgrams are shown in Fig. 8 (*A* and *B*), and the binding parameters were calculated for each glycoprotein. The binding of all glycoproteins except BSM fit best a 1:1 binding model among the fitting models in global analysis. The interaction between bovine thyroglobulin and trypsins was analyzed at concentrations lower than 0.25 μM (Fig. 8, *A* (*panel e*) and *B* (*panel o*)), because bovine thyroglobulin gave fluctuating, irregular-shaped binding curves at concentrations higher than 0.5 μM. The interaction between trypsins and BSM showed box-shaped binding curves suggesting high association and dissociation rates (Fig. 8, *A* (*panel j*) and *B* (*panel t*)) and was analyzed using affinity analysis. The kinetic data of the binding are summarized in Table 1.

Trypsin bound to the glycoproteins possessing *N*-glycans with significantly high affinity, K_A ranging from 10^{10}-10^6 M^{-1}. In contrast, the K_A for BSM was as low as $1–8 \times 10^4$ M^{-1}, indicating very weak interaction with trypsins. The K_A for bovine thyroglobulin binding to both PPT and BPT was 10^{10} M^{-1}, which is the strongest among glycoproteins and equal to that of high affinity antibodies, followed by the K_A of porcine thyroglobulin, $4–5 \times 10^7$ M^{-1}. The high K_A of trypsin for bovine thyroglobulin is attributable to the extremely low dissociation rate constants (k_d) (10^{-7}-10^{-6} s^{-1}) compared with those of other glycoproteins (10^{-4}-10^{-3} s^{-1}), suggesting that thyroglobulins hardly dissociate from trypsin. The K_A of trypsin for bovine thyroglobulin was markedly decreased from 10^{10} to 10^5 (M^{-1}) by α-galactosidase treatment, indicating that α-galactose residues are essential for high affinity binding to trypsin. On the other hand, the K_A of trypsin for porcine thyroglobulins ($4–5 \times 10^7$ M^{-1}) was decreased to 15–20% by treatment with endoglycosidase H or neuraminidase, showing that high-Man types as well as sialyl residues of complex types contribute to the binding. The K_A for fetuin was decreased by *N*-glycosidase F treatment by ~10^{-3}-fold but not by *O*-glycosidase treatment, indicating that the sialylated complex-type *N*-glycans of fetuin contributed absolutely to the binding, but *O*-glycans did not, even if they are sialylated. The results correlated well with the reactivities of trypsin toward intact and glycosidase-modified glycoprotein probes by ELISA.

Effect of Sugars on Enzyme Activity of PPT

As shown in Fig. 9*A*, the sugars that bound to trypsins enhanced the enzyme activity to various degrees, as detected using BAEE and BAPA as substrates. The hydrolytic activity of PPT for BAEE was enhanced by 1.4-fold in 0.2 M methyl-α-D-mannoside and 1.2-fold in methyl-α-D-galactoside but not enhanced in 0.2 M lactose. When we used a slowly hydrolyzable BAPA as the substrate, PPT was activated with 0.2 M methyl-α-D-mannoside and methyl-α-D-galactoside to ~1.2- to 1.4-fold at 300–600 s (Fig. 9*B*). As shown in Fig. 9 (*C–E*) and Table 1, the Lineweaver-Burk plots indicate that the binding of Me-α-Man, and Me-α-galactoside uncompetitively activates PPT with increasing V_{max} by 2.5-fold and K_m by 2- to 2.5-fold, while binding of lactose slightly inhibited PPT noncompetitively and uncompetitively, indicating that the binding of carbohydrates activates the hydrolytic activity to various degrees.

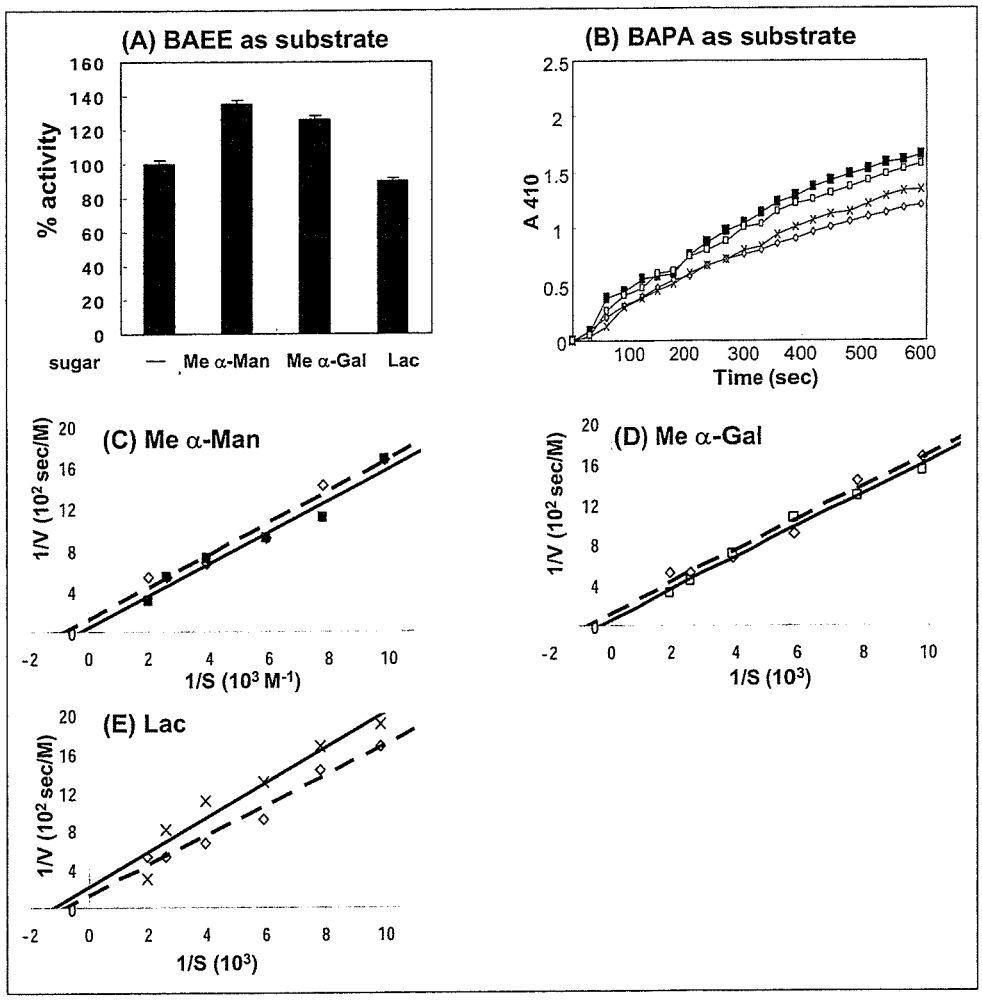

FIGURE 9. **Effect of various sugars on enzyme activity of PPT.** *A*, aliquots (100 μl) of 0.2 M methyl-α-mannoside, methyl-α-galactoside, or lactose, or buffer for the control were added to PPT (2 μg) in the same volume, and the enzyme activity was measured against BAEE as described in the text. Relative activity was expressed as a percentage, taking the control as 100%. *B*, time course of PPT activity in the presence of various sugars. The enzyme activity was measured against BAPA as described in the text in the presence or absence of 0.2 M methyl-α-mannoside (■), methyl-α-galactoside (□), lactose (◇), and control (×). *C–E*, Lineweaver-Burk plots of PPT. PPT activity was measured in the presence (*solid line*) or absence (*dashed line*) of 0.2 M concentrations of various sugars as described in the text and analyzed by a double reciprocal Lineweaver-Burk plot.

TABLE 2

K_m value and V_{max} of PPT activity on effect of various sugars

The enzyme activity was measured in the presence of various sugars (0.2 M) and analyzed by the Lineweaver-Burk plot.

Sugars or glycoprotein	V_{max}	K_m	Mode of effect
	$\times 10^{-3}$ M/s	$\times 10^{-3}$ M	
Control	8.08	1.26	
Me-α-Man	20.7	3.20	Uncompetitive activation
Me-α-Gal	18.1	2.81	Uncompetitive activation
Lac	4.70	0.85	Non- and uncompetitive inhibition

DISCUSSION

This study demonstrates that mammalian pancreatic trypsin commonly binds to glycoproteins possessing *N*-linked glycans by carbohydrate-specific interaction. The sugar-binding specificity of trypsin was shown by the binding with sugar-BP probes and glycolipid analogues to be α-galactosyl, oligomannosyl, and nonreducing terminal α2,6-NeuAc residues (Fig. 1). Trypsin bound to glycoproteins possessing *N*-glycans with very high affinity, reaching 10^{10}-10^6 M^{-1}, whereas it did not bind to BSM (Fig. 4 and Table 1). The binding of glycoprotein probes with trypsin was changed by glycosidase treatments on ELISA and SPR analyses, which coincided well with the sugar-binding specificity indicated by sugar-BP probes. The specificity of the interaction between trypsin and the glycoproteins was proven by inhibition studies with monosaccharides using SPR (Fig. 7) and conclusively demonstrated to be due to the affinity of trypsin for component saccharide residues of the *N*-linked glycans but not by protein-protein interaction.

Treatment of trypsin with soybean trypsin inhibitor and PMSF did not affect the binding to sugar-BP, glycolipid analogues, and glycoprotein probes, and trypsin was noncompetitively and uncompetitively activated toward synthetic substrates, BAEE and BAPA, by the binding of specific sugars (Fig. 9 and Table 2). Therefore, the *N*-glycan recognition of trypsin must be exhibited at a site different from its catalytic site, and activation would be caused by an allosteric effect to make the substrate-binding site more accessible to the substrate and/or by a conformational effect that stabilizes the trypsin molecule against autodegradation, like the stabilizing effect of Ca^{2+} binding (14).

The coating of oligosaccharides on glycoproteins can serve to protect the polypeptide chain from degradation by proteases (3). The contributions of sialylation to the stabilization of glycoprotein against tryptic hydrolysis have been reported for several glycoproteins, including orosomucoid (15) and vitronectin (16). The de-*N*-glycosylation of ovomucoid with trifluoromethanesulfonic acid has been reported to interfere with the inhibitory activity against trypsin and make ovomucoid easily hydrolyzable with trypsin (17). Although the relationship between oligosaccharide structure and the protective function against proteases has been explored for several glycoproteins (18–20), the protecting mechanism achieved by the oligosaccharides has remained unclear. Because the removal of oligosaccharides from a mature protein does not always drastically alter its sensitivity to proteolysis,

some specific interaction between protease and glycoproteins may be involved in regulating protease attack. We found that trypsin sugar-specifically interacts with *N*-linked glycoproteins. The binding of trypsin to the *N*-glycans of glycoprotein would protect the carrier glycoprotein from hydrolysis, at least partially, by topologically restricting the substrate-binding site of trypsin. Deglycosylation of glycoproteins, which diminishes the carbohydrate-specific binding, makes trypsin interact with the peptide moiety of the glycoprotein through the substrate-binding site to hydrolyze it. In this hypothesis, glycosylation at even one site of the polypeptide can significantly affect the proteolysis of the carrier glycoprotein. It is necessary to define the relationship between the structure and position of glycosylation that affects the susceptibility to trypsin to examine the hypothesis.

The binding specificity of trypsin toward carbohydrates was different from that of PPA. Trypsin bound little to *N*-acetyllactosamine and α-GalNAc, which bound well to PPA, and bound to fetuin better than to transferrin (Fig. 4), whereas PPA bound to transferrin better than to fetuin (6). The differences may suggest that the endogenous receptors for trypsin and α-amylase are not identical.

The carbohydrate-binding activity of trypsin was exhibited at a broad pH range with the optimum at pH 8.0, the slightly alkaline pH similar to the pancreatic fluid in the intestinal lumen. Therefore, trypsin may interact with glycoligands in the epithelial surface of the duodenum and intestine *in vivo*, because it is extensively glycosylated with *N*-glycans (21–23) containing α-galactose residues (24). The *N*-glycan-binding activity would play a role in targeting trypsin and concentrating it on the brush-border membrane. Such immobilization of trypsin would enhance the activity and/or elongate the short life span of trypsin by stabilizing it against autodegradation. Because the ability of the duodenum to digest proteins increases rapidly in the cascade of enzyme activations following trypsin activation, the enhancement of trypsin activity would be amplified to increase digestive efficiency exponentially; therefore, the 140% enhancement of trypsin activity measured by using BAEE would be amplified in the duodenum to increase more than 5-fold after the sixth stage. In addition, the binding of trypsin to intestinal epithelium makes the product peptides spatially available as a substrate for the exo-type peptidases that are naturally anchored to the intestinal brush-border membrane. The activated proteinases cooperatively break down dietary proteins to peptides that are subsequently degraded to amino acids by other exo-type peptidases either secreted or expressed in the brush border membrane of epithelial cells in the duodenum and small intestine. Rat aminopeptidase N (EC 3.4.11.2) is one of such glycoproteins with 20% (w/w) carbohydrates that possess unsialylated tri- and tetraantennary complex types as major *N*-glycans (25), which are very similar to the glycans of ovomucoid. A major part of dipeptidylpeptidase IV (EC 3.4.14.5) (26) and peptide transporter-1, a H+/peptide cotransporter responsible for the uptake of small peptides (27), are among the *N*-glycosylated glycoproteins in the small intestine, too. The association of trypsin with this exopeptidase or transporter would enhance the rate of degradation of substrate proteins and peptide absorption by increasing the catalytic efficiency both allosterically and with mass action after. The binding of trypsin to intestinal glycoreceptors may also stimulate exocrine secretion of digestive tract hormones or pancreatic proteins as reported for exogenously administered plant lectins (28). The carbohydrate binding may regulate the reactivity of trypsin with the glycosylated protease-activated receptor 2 depending on the glycosylation state (29) and influence intestinal inflammation, cytoprotection, and cellular motility.

Together with our previous findings on pancreatic α-amylase, carbohydrate-binding activities of macromolecule-degrading enzymes might play essential roles in localization, activation, and stabilization of pancreatic enzymes to achieve efficient digestion. Considering the biological significance of trypsin in the activation of other proteinases and its degradative role in various tissues, the mechanism of modulating tryptic susceptibility by glycosylation of proteins must be elucidated.

REFERENCES

1. Marth, J. D. (1999) in *Essentials of Glycobiology* (Varki, A., Esko, J. R. C., Freeze, H., Hart, G., and Marth, J. D., eds) pp. 85–100, Cold Spring Harbor Laboratory Press, Woodbury, NY
2. Helenius, A., and Aebi, M. (2001) *Science* **291,** 2364–2369
3. Varki, A. (1993) *Glycobiology* **3,** 97–130
4. Chen, J. M., and Ferec, C. (2000) *Pancreas* **21,** 57–62
5. Phillips, M. A., and Fletterick, R. J. (1992) *Curr. Opin. Struct. Biol.* **2,** 713–720
6. Matsushita, H., Takenaka, M., and Ogawa, H. (2002) *J. Biol. Chem.* **277,** 4680–4686
7. Ueda, H., Kojima, K., Saitoh, T., and Ogawa, H. (1999) *FEBS Lett.* **448,** 75–80
8. Laemmli, U. K. (1970) *Nature* **227,** 680–685
9. Azefu, Y., Tamiaki, H., Sato, R., and Toma, K. (2002) *Bioorg. Med. Chem.* **10,** 4013–4022
10. Sato, R., Toma, K., Nomura, K., Takagi, M., Yoshida, T., Azefu, Y., and Tamiaki, H. (2004) *J. Carbohyd. Chem.* **23,** 375–388
11. Schwert, G. W., and Takenaka, Y. (1955) *Biochim. Biophys. Acta* **16,** 570–575
12. Erlanger, B. F., Kokowsky, N., and Cohen W. (1961) *Arch. Biochem. Biophys.* **95,** 271–278
13. Mann, D. A., Kanai, M., Maly, D. J., and Kiessling L. L. (1998) *J. Am. Chem. Soc.* **120,** 10575–10582
14. Abbott, F., Gomez, J. E., Birnbaum, E. R., and Darnall, D. W. (1975) *Biochemistry* **14,** 4935–4943
15. Sharon, N. (1975) *Complex Carbohydrates: Their Chemistry, Biosynthesis and Functions*, pp. 109–117, Addison-Wesley Publishing, Reading, MS
16. Uchibori-Iwaki, H., Yoneda, A., Oda-Tamai, S., Kato, S., Akamatsu, N., Otsuka, M., Murase, K., Kojima, K., Suzuki, R., Maeya, Y., Tanabe, M., and Ogawa, H. (2000) *Glycobiology* **10,** 865–874
17. Gu, J. X., Matsuda, T., Nakamura, R., Ishiguro, H., Ohkubo, I., Sasaki, M., and Takahashi, N. (1989) *J. Biochem. (Tokyo)* **106,** 66–70
18. Gentile, F., and Salvatore, G. (1993) *Eur. J. Biochem.* **218,** 603–621
19. Arnold, U., Schierhorn, A., and Ulbrich-Hofmann, R. (1998) *J. Protein Chem.* **17,** 397–405
20. Ashida, H., Yamamoto, K., and Kumagai, H. (2000) *Biosci. Biotechnol. Biochem.* **64,** 2266–2268
21. Roth, J. (1993) *Histochem. J.* **25,** 687–710
22. Roth, J. (1987) *Biochim. Biophys. Acta* **906,** 405–436
23. Pusztai, A., Ewen, S. W., Grant, G., Peumans, W. J., Van Damme, E. J., Coates, M. E., and Bardocz, S. (1995) *Glycoconj. J.* **12,** 22–35
24. Oriol, R., Barthod, F., Bergemer, A. M., Ye, Y., Koren, E., and Cooper, D. K. (1994) *Transpl. Int.* **7,** 405–413
25. Takasaki, S., Erickson, R. H., Kim, Y. S., Kochibe, N., and Kobata, A. (1991) *Biochemistry* **30,** 9102–9110
26. Erickson, R. H., and Kim, Y. S. (1983) *Biochim. Biophys. Acta* **743,** 37–42
27. Shen, H., Smith, D. E., and Brosius, F. C., 3rd. (2001) *Pediatr. Res.* **49,** 789–795
28. Pusztai, A., and Bardocz, S. (1996) *Trends Glycosci. Glycotechnol.* **8,** 149–165
29. Hollenberg, M. D., and Compton, S. J. (2002) *Pharmacol. Rev.* **54,** 203–217
30. Yamashita, K., Kamerling, J. P., and Kobata, A. (1982) *J. Biol. Chem.* **257,** 12809–12814
31. van Dijk, W., Havenaar, E. C., and Brinkman-van der Linden, E. C. (1995) *Glycoconj. J.* **12,** 227–233
32. Thall, A., and Galili, U. (1990) *Biochemistry* **29,** 3959–3965
33. Ito, S., Yamashita, K., Spiro, R. G., and Kobata, A. (1977) *J. Biochem. (Tokyo)* **81,** 1621–1631
34. Kamerling, J. P., Rijkse, I., Maas, A. A., van Kuik, J. A., and Vliegenthart, J. F. (1988) *FEBS Lett.* **241,** 246–250
35. Tsuji, T., Yamamoto, K., Irimura, T., and Osawa, T. (1981) *Biochem. J.* **195,** 691–699
36. Yamamoto, K., Tsuji, T., Irimura, T., and Osawa, T. (1981) *Biochem. J.* **195,** 701–713
37. Fu, D., and van Halbeek, H. (1992) *Anal. Biochem.* **206,** 53–63
38. Takasaki, S., and Kobata, A. (1986) *Biochemistry* **25,** 5709–5715
39. Berman, E. (1987) *Magn. Reson. Chem.* **25,** 784–789
40. Tsuji, T., and Osawa, T. (1986) *Carbohydr. Res.* **151,** 391–402
41. Toba, S., Tenno, M., and Kurosaka, A. (2000) *Biochem. Biophys. Res. Commun.* **271,** 281–286

Glycobiology vol. 16 no. 7 pp. 651–665, 2006
doi:10.1093/glycob/cwj112
Advance Access publication on April 11, 2006

Identification of disialic acid-containing glycoproteins in mouse serum: a novel modification of immunoglobulin light chains, vitronectin, and plasminogen

Zenta Yasukawa[3,4], Chihiro Sato[1,3,4], Kotone Sano[5], Haruko Ogawa[5], and Ken Kitajima[2,3,4]

[3]Laboratory of Animal Cell Function, Bioscience and Biotechnology Center, and [4]Department of Applied Molecular Biosciences, Graduate School of Bioagricultural Sciences, Nagoya University, Nagoya 464-8601, Japan; and [5]Department of Advanced BioSciences, Graduate School of Humanities and Sciences, Ochanomizu University, Tokyo 112-8610, Japan

Received on January 28, 2006; revised on March 31, 2006; accepted on April 4, 2006

Serum glycoproteins are involved in various biologic activities, such as the removal of exogenous antigens, fibrinolysis, and metal transport. Some of them are also useful markers of inflammation and disease. Although the amount of sialic acid increases following inflammation, little attention has been paid to the presence of linkage-specific epitopes in serum, especially the α2,8-linkage. In a previous study, we demonstrated that four components in mouse serum contain α2,8-linked disialic acid (diSia), based on immunoreactivity with monoclonal antibody 2-4B, which is specific to *N*-glycolylneuraminic acid (Neu5Gc)α2→(8Neu5Gcα2→)$_{n-1}$, $n \geq 2$ [Yasukawa *et al.*, (2005) *Glycobiology*, 15, 827–837]. In this study, we purified three components, 30-, 70-, and 120-kDa gp, and identified them as an immunoglobulin (Ig) light chain, vitronectin, and plasminogen, respectively, using matrix-assisted laser desorption/ionization time-of-flight mass spectroscopy analyses. Modifications of these proteins with α2,8-linked diSia were chemically confirmed by fluorometric C_7/C_9 analyses and mild acid hydrolysates-fluorometric anion-exchange chromatography analyses. We also demonstrated that the IgG, IgM, and IgE light chains are commonly modified with α2,8-linked diSia. In addition, both mouse and rat vitronectin contained diSia, and the amount of disialylation in vitronectin dramatically decreased after hepatectomy. These results indicate that a novel diSia modification of serum glycoproteins is biologically important for immunologic events and fibrinolysis.

Key words: disialic acid/immunoglobulin light chain/plasminogen/serum glycoprotein/vitronectin

[1]To whom correspondence should be addressed; e-mail: chi@agr.nagoya-u.ac.jp
[2]To whom correspondence should be addressed; e-mail: kitjaima@agr.nagoya-u.ac.jp

Introduction

The sialic acids are a family of 9-carbon carboxylated sugars, containing nearly 50 members that are derivatives of *N*-acetylneuraminic acid (Neu5Ac), *N*-glycolylneuraminic acid (Neu5Gc), and deaminoneuraminic acid (2-keto-3-deoxy-D-*glycero*-D-*galacto*-nononic acid) (Angata and Varki, 2002). Sialic acid is an important non-reducing terminal residue in glycoconjugates and is involved in a wide variety of biologic activities in animals (Schauer, 2004). Sometimes, sialic acid links to another sialic acid to form disialic acid (diSia). DiSia is often present in glycolipids and is involved in cell adhesion, cell signaling, and tumor-antigen expression (Nagai and Iwamori, 1995; Sharon and Lis, 1997). Recently, we demonstrated that the α2,8-linked diSia structure is a common carbohydrate antigen not only in glycolipids but also in glycoproteins, using newly developed methods to detect di/oligo/polysialic acid structures in glycoproteins (Sato, Kitajima *et al.*, 1998, Sato *et al.*, 1999, 2000), and identified some molecules as diSia-containing glycoproteins (Sato, 2004).

In serum, sialic acids have an important role in clearance of serum glycoproteins (Drickamer, 1991). Sialic acid residues often cap the terminal galactose residues of serum glycoproteins to prohibit binding to the asialoglycoprotein receptor on hepatocytes (Ashwell and Morell, 1974). Serum glycoproteins are also involved in various biologic activities: immunoglobulins (Igs) and/or complements involved in exclusion of foreign invaders, plasminogen in fibrinolysis, and transferrin and ceruloplasmin in metal transport. They are useful markers of inflammation and disease (Browning *et al.*, 2004; Petersen *et al.*, 2004). The amount of sialic acid in serum is sometimes used as a marker of inflammation because acute-phase proteins such as α_1-acid glycoprotein and α_1-antitrypsin are capped with sialic acid and increase dramatically after induction of inflammation (Sillanaukee *et al.*, 1999). Previously, we focussed on changes in the expression of α2,3-, α2,6-, and α2,8-linked sialic acid glycotopes in serum glycoproteins, especially under inflammatory conditions, using *Maackia amurensis* (specific for Siaα2,3Galβ1,4GlcNAc) and *Sambucus sieboldiana* (specific for Siaα2,6Gal/GalNAc) lectins, and monoclonal antibody 2-4B [mAb.2-4B]), which specifically recognizes Neu5Gcα2→(8Neu5Gcα2→)$_{n-1}$, $n \geq 2$ (Sato, Kitajima *et al.*, 1998). Based on mAb.2-4B immunoreactivity, the presence of diSia was strongly suggested in four components of mouse serum (Yasukawa *et al.*, 2005). To

understand the function of diSia in serum glycoproteins, it is important to identify its carrier proteins. In this study, we purified the mAb.2-4B-immunoreactive 30-, 70-, and 120-kDa gp from mouse serum and identified them using matrix-assisted laser desorption/ionization time-of-flight mass spectroscopy (MALDI-TOF MS) analyses as an Ig κ chain, vitronectin, and plasminogen, respectively. Chemical analysis confirmed that these components contain diSia.

Results

Purification of the mAb.2-4B-immunoreactive molecules, 30-, 70-, and 120-kDa gp from mouse serum and MALDI-TOF MS analyses

In a previous study (Yasukawa *et al.*, 2005), we showed that four components in mouse serum were immunoreactive with mAb.2-4B (Sato, Kitajima *et al.*, 1998) (Figure 1). Specifically, 32-kDa gp was an acute-phase protein during inflammation (Yasukawa *et al.*, 2005) and was identified as carbonic anhydrase II. We developed this antibody using phosphatidylethanolamine-conjugated (Neu5Gc)*n* structure as immunogen. Using (Neu5Gc)*n*-PE (*n* is defined), glycoprotein containing (Neu5Gc)*n* and the periodate-treated antigens, mAb.2-4B was shown to react specifically with (→8Neu5Gcα2→)*n*, (*n* ≥ 2) (Sato, Kitajima *et al.*, 1998; Sato *et al.*, 2000). Based on mAb.2-4B immunoreactivity, other components, 30-, 70-, and 120-kDa gp, are considered to have di/oligoNeu5Gc residues. To identify these glycoproteins, we purified them from mouse serum as described below.

Purification and identification of the 30- and 120-kDa gp. The 30- and 120-kDa gp were salted out from mouse serum with 50% $(NH_4)_2SO_4$. The proteins in the 50% $(NH_4)_2SO_4$ precipitate were separated by Sephacryl S-100 gel filtration chromatography. The elution was monitored by absorbance at 280 nm, sodium dodecyl sulfate–polyacrylamide gel electrophoresis (SDS–PAGE) followed by Coomassie brilliant blue (CBB) staining, and immunoblotting with mAb.2-4B (Figure 2a). The 30-kDa gp was detected in fractions 41–45, and the 120-kDa gp was detected in fractions 45–49. Fractions 39–45 were pooled and further separated by DEAE-Toyopearl 650 M anion-exchange chromatography with a linear NaCl gradient. The elution was monitored as described in Figure 2a. The 30-kDa gp was detected in fractions 63 and 81, whereas the 120-kDa gp was detected in fraction 63. The CBB-stained band of the 30-kDa gp in fraction 81 and the 120-kDa gp in fraction 63 was excised from the polyacrylamide gel and destained. The gels were digested with trypsin, and the obtained peptides were analyzed by MALDI-TOF MS analyses (Figure 2c for the 30-kDa gp and Figure 2e for the 120-kDa gp). The observed peaks at m/z 940.43, 990.54, 1361.64, and 2176.11 from the 30-kDa gp were considered to come from the Ig light-chain κ-constant region by peptide mass fingerprinting followed by database searches (Figure 2d and Table I). All the observed peptide sequences were confirmed by tandem mass spectrometry (MS/MS) analyses (Table I, boldface-type sequences, data not shown). The observed sequences covered 32% of the Ig light-chain κ-constant region sequence (CAC20700). From the tryptic digests of the 120-kDa gp, 10 discrete peaks were obtained by MALDI-TOF MS analyses (Figure 2e), and these peak components were determined to be parts of plasminogen using peptide mass fingerprinting followed by database searches (Figure 2f and Table I). Of 10 sequences, six were also confirmed by MS/MS analyses (Table I, boldface-type sequences, data not shown). The observed sequences covered 13% of the plasminogen sequence (AAA50168).

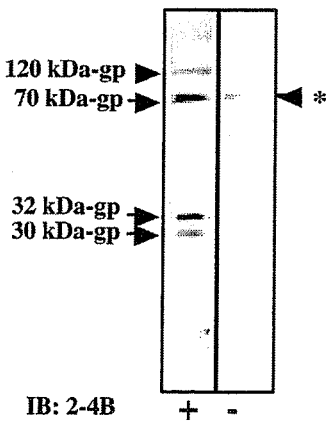

Fig. 1. The monoclonal antibody 2-4B (mAb.2-4B)-immunoreactive glycoproteins in mouse serum. Mouse serum (0.5 μL; 15 μg as protein) was subjected to sodium dodecyl sulfate–polyacrylamide gel electrophoresis/electroblotting on polyvinylidene difluoride membrane. The membrane was immunostained with (+) or without (–) mAb.2-4B, which is specific to Neu5Gcα2→(8Neu5Gcα2→)$_{n-1}$, (*n* ≥ 2) structure as a primary antibody. The mAb.2-4B-reactive glycoproteins are indicated by the arrows on the left. Asterisk indicates non-specific binding in the control blots, which lacked the primary antibodies.

Purification of the 70-kDa gp. The 70-kDa gp was salted out with 70% $(NH_4)_2SO_4$ using the supernatant derived from the 50% $(NH_4)_2SO_4$ solution of the inflamed mouse sera, as described in *Materials and Methods*. The precipitate was separated by Sephacryl S-100 gel filtration chromatography. The elution was monitored by absorbance at 280 nm (Figure 3a) and by SDS–PAGE followed by CBB staining and western blotting (data not shown). Fractions 44–61, which contained the mAb.2-4B-immunoreactive 70-kDa gp, were pooled and further separated by DEAE-Toyopearl 650 M anion-exchange chromatography and eluted by stepwise elution. The elution was monitored by absorbance at 280 nm (Figure 3b, left panel) and by SDS–PAGE followed by CBB staining and western blotting (data not shown). The 70-kDa gp was purified to homogeneity as a single band (Figure 3b, CBB) in the fractions eluted by 1.0 M NaCl, and the 70-kDa band was immunostained with mAb.2-4B (Figure 3b, 2-4B). The CBB-stained band of the 70-kDa gp was excised from the gel, destained, and digested with trypsin. The peptides were analyzed by MALDI-TOF MS (Figure 3c). The peptide mass fingerprints obtained by MALDI-TOF MS followed by database searches identified the 70-kDa gp as vitronectin (Figure 3d and Table I). Of nine sequences, four were also confirmed by MS/MS analyses (Table I, boldface-type sequences, data not shown). The observed sequences covered 23% of the vitronectin sequence (AAA40558).

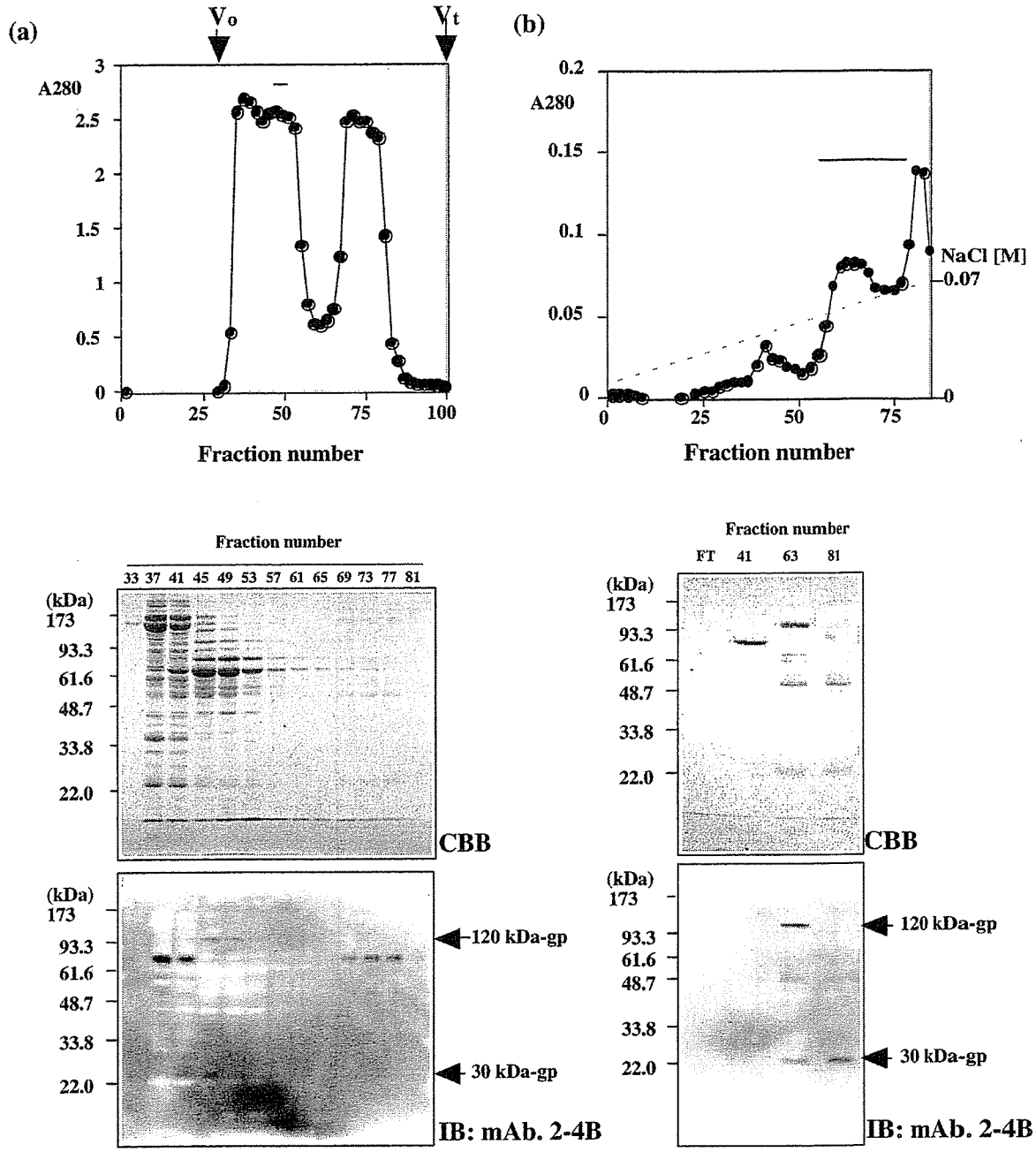

Fig. 2. Purification of the 30- and 120-kDa gp from normal mouse serum and MALDI-TOF MS analyses of their tryptic digest. (**a**) Sephacryl S-100 chromatography of 50% $(NH_4)_2SO_4$ precipitate of normal mouse serum (upper panel). Mouse serum was subjected to ammonium sulfate precipitation as described in *Materials and Methods*. The 50% $(NH_4)_2SO_4$ precipitate was applied to the column (1.3 × 75 cm) and eluted with 0.01 M NaCl in 10 mM Tris–HCl (pH 8.0). Elution was monitored by absorbance at 280 nm (V_0, void volume; V_t, total volume). Fractions were also monitored SDS–PAGE CBB staining (denoted as CBB, middle panel) and western blotting with mAb.2-4B (IB: 2-4B, lower panel). Aliquots (1 μL) of fractions 33–81 were loaded on a 10% polyacrylamide gel. Positions of the molecular mass markers are indicated on the left. The mAb.2-4B-immunoreactive proteins at 30- and 120-kDa gp-containing fractions (fractions 39–45) indicated by the bars were pooled. (**b**) DEAE-Toyopearl 650 M chromatography of the major 30- and 120-kDa gp-containing fractions in (**a**). The pooled fraction was applied to a DEAE-Toyopearl 650 M (Cl^- form; column size 1.2 × 17 cm) and eluted with a linear gradient of NaCl (0.01–0.07 M) in 0.01 M Tris–HCl (pH 8.0) (upper panel) as described in *Materials and Methods*. The NaCl concentration is shown by the dotted line. Elution profile was monitored by the absorbance at 280 nm. SDS–PAGE/CBB staining (denoted as CBB, middle panel) and western blotting with mAb.2-4B (IB: 2-4B) (lower panel) of fractions 41, 63, and 81 eluted from DEAE-Toyopearl 650 M chromatography were loaded on 10% polyacrylamide gel. Positions of the molecular mass markers are indicated on the left. The 30-kDa gp-containing fractions (fractions 56–79 at 0.050–0.065 M NaCl) were pooled as indicated by the bars. (**c**) MS spectrum (reflectron mode) of a tryptic digest of the 30-kDa gp. The 30-kDa gp band seen in (**b**) at fraction 81 was excised, digested in gel by trypsin, and analyzed by MALDI-TOF MS as described in *Materials and Methods*. (**d**) Sequence of the immunoglobulin light-chain κ-constant region (CAC20700). The putative sequences of observed peptides are summarized in Table I and are given in boldface type. (**e**) MS spectrum (reflectron mode) of a tryptic digest of the 120-kDa gp. The 120-kDa gp band observed in (**b**) at fraction 63 was excised, digested in gel by trypsin, and analyzed by MALDI-TOF MS as described in *Materials and Methods*. (**f**) Plasminogen sequence (AAA50168). The putative sequences of observed peptides are summarized in Table I and are underlined in boldface type.

(c)

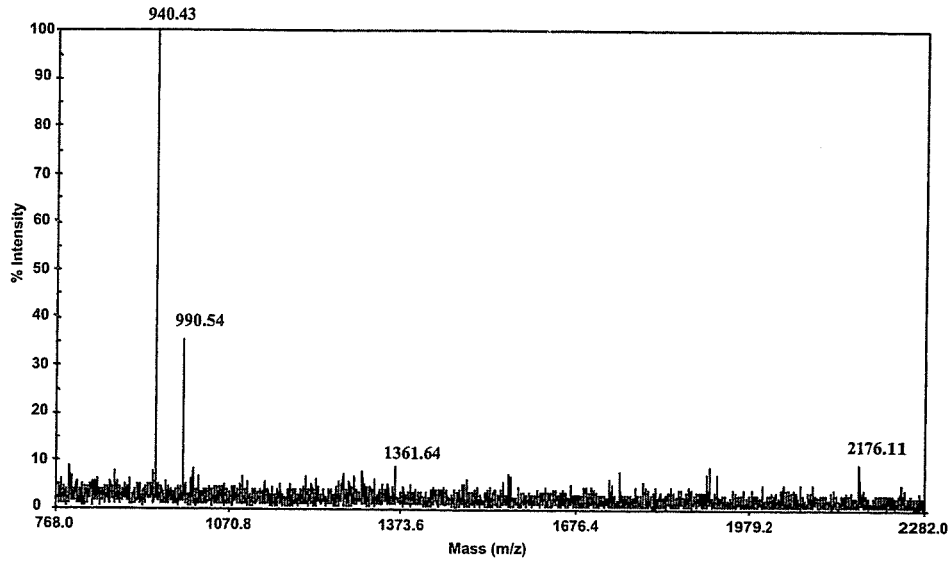

(d)

```
  1 ADAAPTVSIF PPSSEQLTSG GASVVCFLNN FYPKDINVK W KIDGSERQNG
  5 VLNSWTDQDS KDSTYSMSST LTLTKDEYER  HNSYTCEATH KTSTSPIVKS
101 FNRNEC
```

(e)

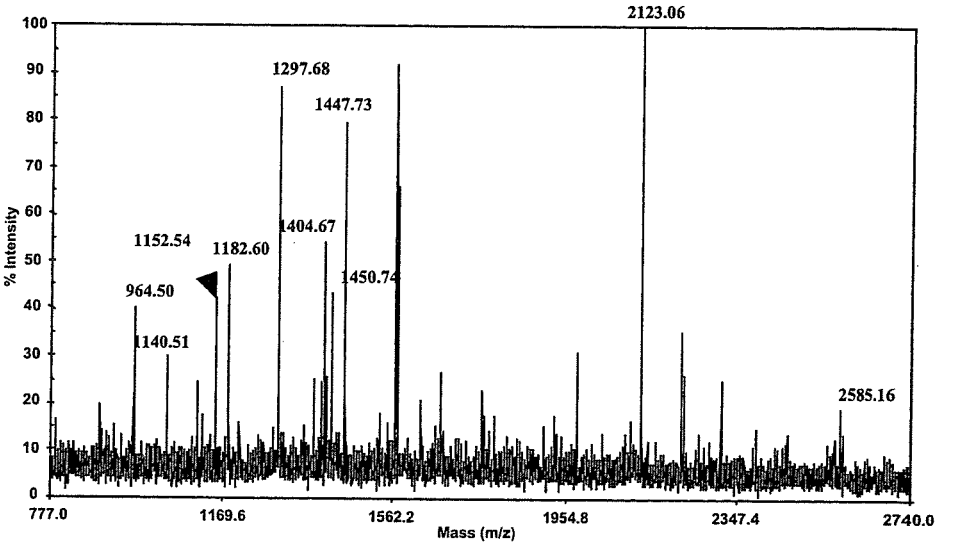

(f)

```
  1 MDHKEVILLF LLLLKPGQGD SLDGYISTQG ASLFSLTKK Q LAAGGVSDCL
 51 AKCEGETDFV CRSFQYHSKE QQCVIMAENS KTSSIIRMRD VILFEKRVYL
101 SECKTGIGNG YRGTMSRTKS GVACQKWGAT FPHVPNYSPS THPNEGLEEN
151 YCRNPDNDEQ GPWCYTTDPD KRYDYCNIPE CEEECMYCSG EKYEGKISKT
201 MSGLDCQAWD SQSPHAHGYI PAKFPSKNLK MNYCHNPDGE PRPWCFTTDP
251 TKRWEYCDIP RCTTPPPPPS PTYQCLKGRG ENYRGTVSVT VSGKTCQR WS
301 EQTPHRHNRT PENFPCKNLE ENYCRNPDGE TAPWCYTTDS QLRWEYCEIP
351 SCESSASPDQ SDSSVPPEEQ TPVVQECYQS DGQSYRGTSS TTITGKK CQS
401 WAAMFPHRHS KTPENFPDAG LEMNYCRNPD GDKGPWCYTT DPSVR WEYCN
451 LKRCSETGGS VVELPTVSQE PSGPSDSETD CMYGNGKDYR GK TAVTAAGT
501 PCQGWAAQEP HRHSIFTPQT NPRADLEKNY CRNPDGDVNG PWCYTTNPRK
551 LYDYCDIPLC ASASSFECGK PQVEPKKCPG RVVGGCVANP HSWPWQISLR
601 TRFTGQHFCG GTLIAPEWVL TAAHCLEKSS RPEFYKVILG AHEEYIRGLD
651 VQEISVAKLI LEPNNRDIAL LKLSRPATIT DKVIPACLPS PNYMVADRTI
701 CYITGWGETQ GTFGAGRLKE AQLPVIENK V CNRVEYLNNR VKSTELCAGQ
751 LAGGVDSCQG DSGGPLVCFE KDKYILQGVT SWGLGCARPN KPGVYVRVSR
801 FVDWIEREMR NN
```

Fig. 2. continued

Table I. Summary of the peptide sequences of peptide fragments obtained by MALDI-TOF MS analysis of the 30, 70, and 120-kDa gp purified from mouse serum

	Peptide sequence	MH^+ observed	Mr theoretical	Delta (Da)	Sequence coverage (%)
30-kDa gp	**WKIDGSER** (40–47)	990.54	989.49	0.04	32
	HNSYTCEATHK (81–91)	1361.64	1360.58	0.05	
	HNSYTCEATHKTSTSPIVK (81–99)	2175.11	2174.04	0.06	
	SFNRNEC (100–106)	940.43	939.39	0.03	
70-kDa gp	CTQGFMASKK (28–37)	1171.45	1170.55	–0.11	23
	GQYCYELDETAVRPGYPK (176–193)	2159.88	2159.00	–0.12	
	LIQDVWGIEGPIDAAFTR (194–211)	2000.91	2000.04	–0.14	
	TYLFK (218–222)	671.96	670.37	0.58	
	GSQYWR (223–228)	796.29	795.36	–0.08	
	FEDGVLDPGYPR (229–240)	1364.53	1363.64	–0.12	
	SSDGAREPQFISR (323–335)	1449.58	1448.70	–0.13	
	NWHGVPGKVDAAMAGR (336–351)	1665.69	1664.82	–0.13	
	IYVTGSLSHSAQAK (352–365)	1461.65	1460.76	–0.12	
120-kDa gp	QLAAGGVSDCLAKCEGETDFVCR (40–62)	2585.16	2584.17	–0.02	13
	WEYCDIPR (254–261)	1152.54	1151.51	0.03	
	WSEQTPHR (299–306)	1040.51	1039.48	0.02	
	WSEQTPHRHNR (299–309)	1447.73	1446.69	0.03	
	CQSWAAMFPHR (398–408)	1404.67	1403.62	0.04	
	WEYCNLKR (446–453)	1182.60	1181.57	0.03	
	TAVTAAGTPCQGWAAQEPHR (493–512)	2123.06	2122.00	0.05	
	HSIFTPQTNPR (513–523)	1297.68	1296.66	0.02	
	VCNRVEYLNNR (730–740)	1450.74	1449.71	0.02	
	FVDWIER (801–807)	964.50	963.48	0.01	

Boldface-type sequences were confirmed by MS/MS analyses.

MALDI-TOF MS analyses indicated that 30-, 70-, and 120-kDa gp mAb.2-4B-immunoreactive components were an Ig light chain, plasminogen, and vitronectin, respectively. To confirm these results, we purified these components from mouse serum by conventional methods and analyzed them for the presence of di/oligosialic acid using chemical analyses.

Affinity purification of the mouse Igs and demonstration of the presence of diSia

The partially purified 30-kDa gp obtained after DEAE-Toyopearl 650 M chromatography (Figure 2b) was applied to a Protein G-Sepharose column. After washing, Igs bound to the Protein G-Sepharose column were eluted with 50 mM diethylamine–HCl (pH 11.5). The purified IgGs were analyzed by western blotting using mAb.2-4B. The mAb.2-4B-positive 30-kDa gp(s) were bound to the Protein G-Sepharose column, which specifically traps the Fc region of IgG, and recovered in the diethylamine-eluted fraction (Figure 4a, elute). In SDS–PAGE/CBB analysis, the 30-kDa band moved up to the 170-kDa band under non-reducing conditions (data not shown). These findings together with the results obtained from MALDI-TOF MS (Figure 2c and d; Table I) confirmed that the 30-kDa gp is the IgG light chain.

To demonstrate the presence of diSia in the 30-kDa gp, we analyzed the purified IgG fraction by mild acid hydrolysis-fluorometric anion-exchange chromatography analysis and the fluorometric C_7/C_9 analysis. First, we analyzed the mild acid hydrolysate of the 30-kDa gp, which was labeled with a fluorescent reagent using anion-exchange chromatography. A Neu5Gc dimer was clearly observed, and higher oligomers were not observed (Figure 4b, middle panel). Then, we performed the fluorometric C_7/C_9 analysis. As summarized in Table II, C_9-Neu5Gc, which indicates the presence of internal sialic acid, was in the IgG fraction with a molar ratio of C_9-Neu5Gc to C_7-Neu5Gc of 0.09, suggesting that theoretically, ~9% of the sialic acid present on the molecule exists as diSia. These results indicate that the Ig light chain has diNeu5Gc residues. To determine the difference among the Ig classes or IgG subclasses, we analyzed a wide variety of monoclonal Igs. The light chains of IgG1, 2a, and 3, and other Ig classes, IgE and IgM, were immunostained with mAb.2-4B (Figure 4c, upper panel). To exclude the possibility of the non-specific binding of the secondary antibody, we used biotinylated mAb.2-4B and detected it with an avidin–biotin–peroxidase complex system. The same result obtained in Figure 4c was observed (data not shown). These data strongly indicate that the Ig light chains all contain the diNeu5Gc residues.

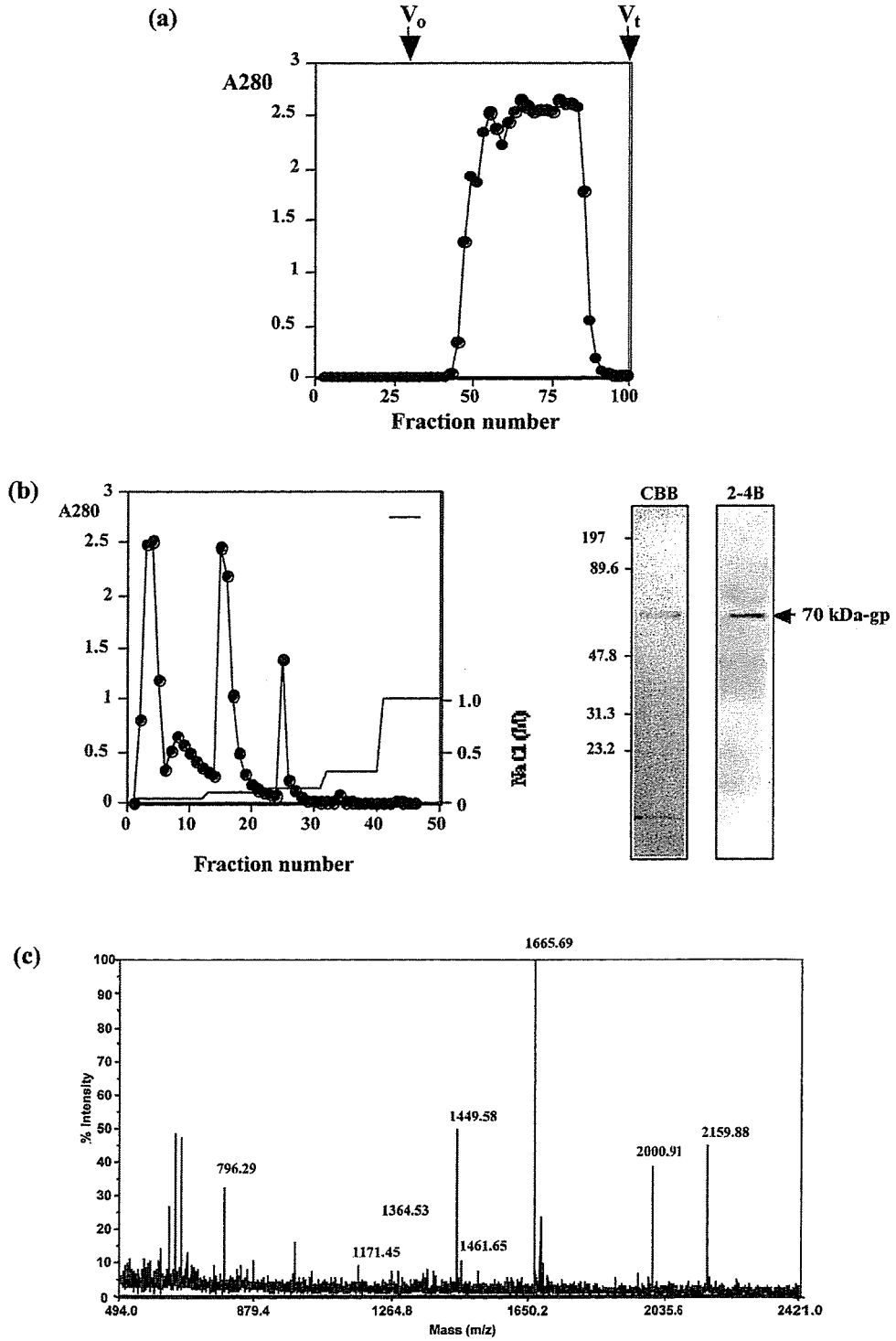

Fig. 3. Purification of the 70-kDa gp and MALDI-TOF MS analyses of its tryptic digest. (**a**) Sephacryl S-100 chromatography of 50% $(NH_4)_2SO_4$ pre itate of inflamed mouse serum. Mouse serum was subjected to ammonium sulfate precipitation as described in *Materials and Methods*. The 50% $(NH_4)_2SO_4$ precipitate was applied to the column (1.3 × 75 cm) and eluted with 0.05 M NaCl in 50 mM Tris–HCl (pH 8.0). The elution profile was monitored by the absorbance at 280 nm and SDS–PAGE CBB and western blot using mAb. 2-4B (V_0, void volume; V_t, total volume). Major 70-kDa gp-containing fractions (fractions 61–80) indicated by the bars were pooled. (**b**) DEAE-Toyopearl 650 M chromatography of the major 70-kDa gp-containing fraction in (**a**). The pooled fraction was applied to a DEAE-Toyopearl 650 M (Cl^- form; column size 1.0 × 24 cm) and eluted with discontinuous NaCl gradients in 0.05 M Tris–HCl (pH 8.0) as described in *Materials and Methods*. The NaCl concentration is shown by the line withou symbol. The elution profile was monitored by the absorbance at 280 nm (left panel). The 70-kDa gp-containing fractions (fractions 42–44 at 1.0 M Na were pooled as indicated by the bars, and the pooled fraction was examined by SDS–PAGE/CBB staining (denoted as CBB) and western blotting usin mAb.2-4B (2-4B). (**c**) Positions of the molecular mass markers are indicated on the left. (**c**) MS spectrum (reflectron mode) of a tryptic digest of the 70-k gp. The 70-kDa gp band observed in (**b**) was excised, digested in gel with trypsin, and analyzed by MALDI-TOF MS as described in *Materials and Methods*. (**d**) Vitronectin sequence (AAA40558). The putative sequences of observed peptides are summarized in Table I and are given in boldface type

(d)

```
  1 MAPLRPFFIL ALVAWVSLAD QESCKGRCTQ GFMASKKCQC DELCTYYQSC
 51 CADYMEQCKP QVTRGDVFTM PEDDYWSYDY VEEPKNNTNT GVQPENTSPP
101 GDLNPRTDGT LKPTAFLDPE EQPSTPAPKV EQQEEILRPD TTDQGTPEFP
151 EEELCSGKPF DAFTDLKNGS LFAFRGQYCY ELDETAVRPG YPKLIQDVWG
201 IEGPIDAAFT RINCQGKTYL FKGSQYWRFE DGVLDPGYPR NISEGFSGIP
251 DNVDAFALPA HRYSGRERVY FFKGKQYWEY EFQQQPSQEE CEGSSLSAVF
301 EHFALLQRDS WENIFELLFW GRSSDGAREP QFISRNWHGV PGKVDAAMAG
351 RIYVTGSLSH SAQAKKQKSK RRSRKRYRSR RGRGHRRSQS SNSRRSSRSI
401 WFSLFSSEES GLGTYNNYDY DMDWLVPATC EPIQVYFFSG DKYYRVNLRT
451 RRVDSVNPPY PRSIAQYWLG CPTSEK
```

Fig. 3. continued

Affinity purification of the mouse plasminogen and demonstration of the presence of di/oligoNeu5Gc

The 120-kDa gp that was specifically immunostained with mAb.2-4B was strongly indicated to be plasminogen by MALDI-TOF MS analyses (Figure 2e and Table I). A lysine-coupled column can be used to purify plasminogen (Edelberg *et al.*, 1990). Thus, normal mouse serum was applied to a lysine-coupled column. After washing, plasminogen was eluted with 300 mM phosphate buffer and 0.1 M 6-aminohexanoic acid in 100 mM phosphate buffer (pH 7.4). SDS–PAGE/CBB staining indicated that the plasminogen was highly purified (Figure 5, lanes 4 and 5), and western blot analysis of each fraction using mAb.2-4B demonstrated that the purified plasminogen contained the di/oligoNeu5Gc structure (Figure 5a, IB: 2-4B). To confirm the presence of diSia chemically, we analyzed plasminogen by mild acid hydrolysis-fluorometric anion-exchange chromatography. The diNeu5Gc structure was observed and higher oligomeric structures were not observed Figure 5b), although the amount of the diSia was not so large as that of IgGs. Then, we analyzed the plasminogen by the fluorometric C_7/C_9 analyses to confirm the presence of diSia (Table II). The ratio of C_9- to C_7-Neu5Gc residues suggested that 3% of the terminal end of the glycan chains were disialylated. The fact that the ratio was lower than that of IgG consists of the observation of the smaller diNeu5Gc peak derived from plasminogen than that from IgGs (Figure 4b). These findings clearly indicated that the mAb.2-4B-immunoreactive 120-kDa gp was plasminogen and that it contains the diNeu5Gc structure.

Affinity purification of mouse vitronectin and demonstration of the presence of diSia

Mouse vitronectin purified using a heparin column as described in *Materials and Methods* was immunostained with mAb.2-4B (data not shown). Based on the MALDI-TOF MS results shown in Figure 3 and Table I, we confirmed that the 70-kDa gp immunostained with mAb.2-4B was vitronectin. To demonstrate the diSia structure chemically, we analyzed the vitronectin by mild acid hydrolysis-fluorometric anion-exchange chromatography. The diNeu5Gc structure was clearly observed, and higher oligomeric structures were not observed (Figure 6a, middle panel). Furthermore, the fluorometric C_7/C_9 analysis of mouse vitronectin also showed the presence of C_9-Neu5Gc-DMB (Table II). The ratio of C_9- to C_7-Neu5Gc of 0.2 indicates that 20% of the terminal end of the sialyl glycan chain in mouse vitronectin is the diNeu5Gc structure. These immunochemical and chemical results clearly demonstrated that mouse vitronectin is modified by di/oligoNeu5Gc. The sialic acid detected in mouse vitronectin was exclusively Neu5Gc (Table II). To determine the difference between species, we also analyzed rat vitronectin. Purified rat vitronectin from serum was also immunostained with mAb.S2-566, which specifically recognizes the Neu5Acα2,8Neu5Acα2,3Gal structure (Figure 6b). The acid hydrolysis-anion exchange fluorometric high-performance liquid chromatography analyses showed that rat vitronectin has the diNeu5Ac structure, and higher oligoNeu5Ac structures were not observed (Figure 6c). These findings indicate that the diSia structure is present in rat vitronectin. Vitronectin is a multifunctional glycoprotein (McKeown-Longo and Panetti, 1996), and sialylation and *N*-glycosylation of vitronectin change markedly in partially hepatectomized rat (Uchibori-Iwaki *et al.*, 2000). Thus, we examined whether disialylation is altered by partial hepatectomy in rat. The purified vitronectin derived from the sera of normal, sham-operated, and partially hepatectomized rats were analyzed to determine the amount of protein by silver staining or the amount of diSia by immunostaining with mAb.S2-566 (Figure 6d), and the ratio of the amounts of diNeu5Ac to that of protein was quantified densitometrically (Figure 6e). Compared with normal rat vitronectin, the amount of diSia in sham-operated rat vitronectin decreased to 65% and that in partially hepatectomized rat vitronectin dramatically decreased to 30% (Figure 6e). These results demonstrate that the diSia structure in vitronectin changes following hepatectomy.

Discussion

In mouse serum, four components, a 30-, 32-, 70-, and 120-kDa gp, were immunoreactive with mAb.2-4B, which

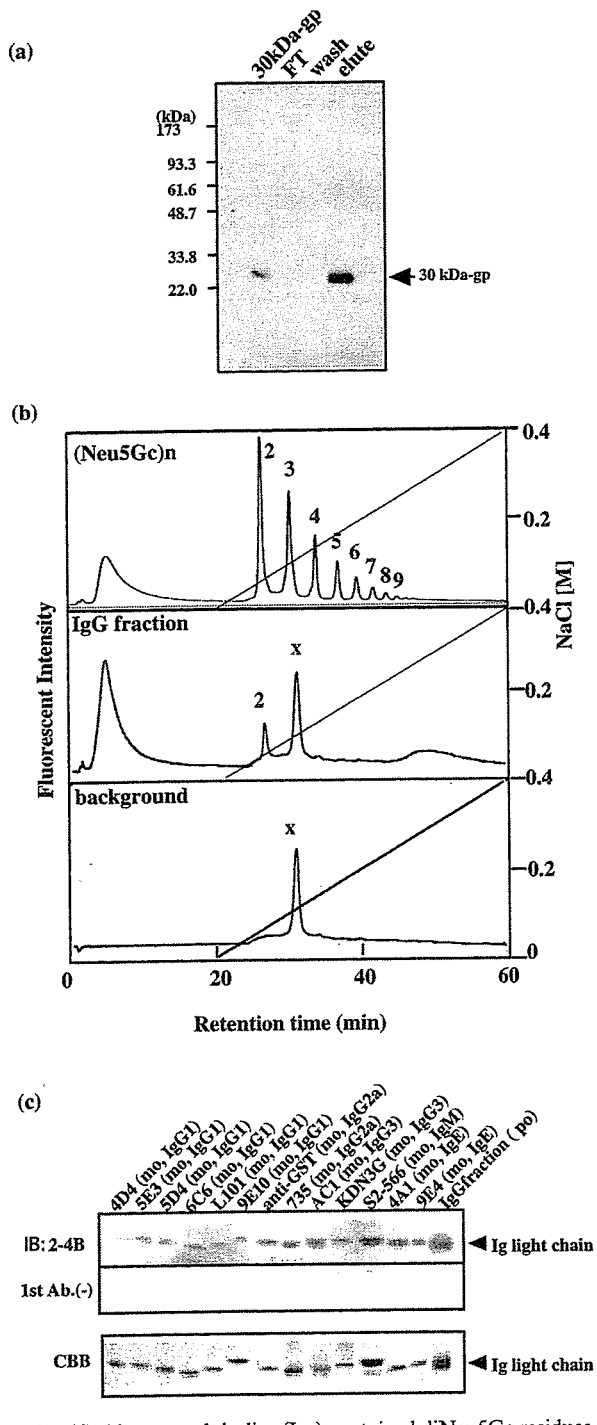

Fig. 4. Purified immunoglobulins (Igs) contained diNeu5Gc residues. (**a**) Protein G-Sepharose chromatography of the 30-kDa gp-containing fractions in Figure 2b. The fraction was applied to a Protein G-Sepharose column (0.7 mL) and eluted as described in *Materials and Methods*. The 30-kDa gp-containing fractions (1 μg as bovine serum albumin [BSA], 30-kDa gp), flow-through fraction (FT), wash fraction (Wash), and eluate fraction (Elute) were analyzed by western blotting using mAb.2-4B as a primary antibody. Positions of the molecular mass markers are indicated on the left. (**b**) Resource Q anion-exchange chromatography of di/oligo/polyNeu5Gc–DMB. Upper panel: α2→8-linked di/oligo/polyNeu5Gc derived from mild acid hydrolysates of polysialoglycoprotein [(Neu5Gc)*n*, 2 μg as Neu5Gc] labeled with DMB were applied to a Resource Q anion-exchange column (1 mL, Cl^- form). The column was eluted with 10 mM Tris–HCl (pH 8.0) with a gradient from 0–0.4 M NaCl as indicated by the thin line. The elution was monitored by a fluorescence detector (excitation 373 nm, emission 448 nm). The number at each peak represents the degree of polymerization (DP). Middle panel: IgG fraction, 30-kDa gp, (22 μg as BSA) was treated with 0.01 N trifluoroacetic acid at 50°C for 1 h, and released sialyloligomer was labeled with DMB. Labeled sialyloligomer was applied to a high-performance liquid chromatograph as described above. The peak labeled 'x' indicates an unidentified peak that was also detected in the background (bottom panel). (**c**) Western blot analyses of various Igs. Monoclonal Igs (0.3–5 μg as BSA/lane) were subjected to SDS–PAGE/CBB staining (denoted as CBB) and western blotting with mAb.2-4B (IB: 2-4B) or without primary antibody [1st antibody (-)]. mo, monoclonal; po, polyclonal. IgG fraction obtained from mouse serum was also analyzed (IgG fraction).

specifically recognizes the di/oligoNeu5Gc structure (Yasukawa *et al.*, 2005). Our ultimate goal is to determine the function of disialylation in these molecules, and as a first step, we identified the protein components of these molecules in this study. Recently, we identified the 32-kDa gp as carbonic anhydrase II and demonstrated that it is an acute-phase inflammatory protein (Yasukawa Z *et al.*, in preparation). We purified three other mAb.2-4B-immunoreactive components from mouse serum using several chromatographic steps. MALDI-TOF MS analyses demonstrated that the 30-, 70-, and 120-kDa gp were an Ig light chain, vitronectin, and plasminogen, respectively.

Ig light chains were purified from mouse serum, and this glycoprotein was confirmed by three methods to have diSia. One method was immunoblotting using the anti-di/oligoNeu5Gc antibody, mAb.2-4B. The other two were chemical methods. We observed diNeu5Gc residues by anion-exchange chromatography after 1,2-diamino-4,5-methylenedioxybenzene (DMB) labeling of mild acid hydrolysates of Ig (Figure 4b). The fluorometric C_7/C_9 analyses of purified Ig also showed that ~9% of the terminal sialylglycan chains were disialylated based on the ratio of C_9 to C_7 of Neu5Gc (Table II). The amount of Neu5Ac was 3% that of Neu5Gc, and Neu5Ac was also present as diSia according to the ratio of C_9- to C_7-Neu5Ac (Table II). The presence of sialic acid residues, especially in the mouse light-chain Ig fraction, but not in the heavy-chain fraction, and the findings that IgM and IgE as well as IgG light chains were modified with diSia (Figure 4c) suggest that disialylation is important for the biologic processes of Igs. It is widely reported that IgG contains 2.3 *N*-linked biantennary oligosaccharide chains per molecule in mice (Mizuochi *et al.*, 1987; Raju *et al.*, 2000), and two of these represent the conserved glycosylation sites at Asn-297 in each of the two heavy-chain C_H2 domains of the Fc portion, and the remainder is found in the hypervariable regions of the Fab section with the frequency and position dependent on the chance occurrence of the *N*-glycosylation consensus sequence (Asn-Xaa-Thr/Ser). (Parekh *et al.*, 1985; Mizuochi *et al.*, 1987). Variations in the *N*-glycosylation of IgG molecules at one conserved site, Asn-297, in the Fc region can directly modulate Fc-receptor recognition and effector functions (Dwek *et al.*, 1995; Lund *et al.*, 1995, 1996; Wright and Morrison, 1998). *O*-glycosylation in the Fc portion has also been detected in two mouse monoclonal IgG2a antibodies in dot blot experiments using lectins (Coco-Martin *et al.*, 1992). Approximately 40% of the heavy chains of the mouse IgG2b antibodies are *O*-glycosylated at

Table II. Fluorescent C_7/ C_9 analyses of the 30-, 70-, and 120-kDa gp

	Neu5Gc			Neu5Ac		
Sia species	C_9[a] (mol/mol)	C_7 (mol/mol)	C_9/C_7	C_9[a] (mol/mol)	C_7 (mol/mol)	C_9/C_7
30-kDa gp	0.011	0.13	0.09	0.0023	0.0022	1.0
70-kDa gp	0.38	2.2	0.2	Trace	Trace	
120-kDa gp	0.010	0.31	0.03	0.0036	0.017	0.2

Neu5Gc, *N*-glycolylneuraminic acid.
[a]C_9 indicates internal sialic acid via the α2,8-linkage.

Thr-221A in the hinge region, and *O*-glycosylation might be involved in protease resistance (Kim *et al.*, 1994). *O*-glycosylation of the IgG1 light chain is reported on a chimeric antibody (cMu-9–1) (Krishnan *et al.*, 1999). In the present study, we first found that mouse Ig light chains contained diNeu5Gc residues. Because of the ubiquitous presence of diSia in Ig light chains, it might be useful to examine the presence of diSia in Bence-Jones protein, which is secreted into urine due to an imbalance in the amounts of heavy and light chains in plasma cells (Bradwell *et al.*, 2003; Miller *et al.*, 2004). It is important to examine the presence of diSia on such Igs derived during disease states.

The 120-kDa gp was identified as plasminogen, and this glycoprotein also contained diSia in mouse serum. In human serum, plasminogen is present in two major glycoforms, plasminogen 1, which possesses an *N*-linked high mannose-type carbohydrate chain at Asp-289 and an *O*-linked carbohydrate chain at Thr-345, and plasminogen 2, which contains an *O*-linked glycan at Thr-345 (Hayes and Castellino, 1979a; Davidson and Castellino, 1991; Pirie-Shepherd *et al.*, 1997). The *O*-linked carbohydrate chain at Thr-345 is Neu5Acα2→3Galβ1→3GalNAc (Hayes and Castellino, 1979b; Davidson and Castellino, 1991). Plasminogen 2 can be separated into at least six glycoforms according to the Neu5Ac content by isoelectric focusing electrophoresis (Siefring and Castellino, 1974; Gonzalez-Gronow *et al.*, 1990). The Neu5Ac content of plasminogen 2 varies from 1.3 to 13.7 mol/mol protein (Pirie-Shepherd *et al.*, 1995), suggesting the presence of a sialyloligo/polymer. Each glycoform isolated by two dimensional-PAGE of plasminogen 2 displays markedly different kinetic behaviors when activated with tissue-plasminogen activator, urinary-type plasminogen activator, and streptokinase (Pirie-Shepherd *et al.*, 1995, 1996). In this study, mouse plasminogen was shown to have diSia, and this glycoform of plasminogen might regulate tissue plasminogen activator, urinary-type plasminogen activator, and streptokinase.

Vitronectin in mouse and rat also has diSia (Figure 6a and c). Vitronectin is a multifunctional adhesive glycoprotein that originates mainly in hepatocytes and circulates in the blood stream at high concentrations (0.2 mg/mL in humans) (Uchibori-Iwaki *et al.*, 2000). Vitronectin regulates the blood systems related to protease cascades, such as cell lysis, by complement, coagulation, and fibrinolysis (Tomasini and Mosher, 1990; Preissner, 1991). Vitronectin is also found in the extracellular matrix of most tissues and is considered to have a role in cell adhesion, cellular motility, and matrix remodeling. Tissue vitronectin is considered to be present as an active multimeric form, and interactions with various matrix ligands, such as various types of integrins on the cell surfaces, Type-1 plasminogen activator inhibitor, and urokinase receptors, to regulate pericellular proteolysis (McKeown-Longo and Panetti, 1996; Seiffert, 1997; Preissner and Seiffert, 1998), are responsible for these functions. Vitronectin can also bind to various types of collagen through its conformational transition from the native inactive form to an active form (Gebb *et al.*, 1986; Ishikawa-Sakurai and Hayashi, 1993; Izumi *et al.*, 1998). Vitronectins from various animals (human, horse, porcine, bovine, rabbit, and chicken) react with several lectins (*Canavalia ensiformis*, *Triticum vulgare*, *Allomyrina dichotoma*, *Ulex europeaeus*, *Lens culinaris* agglutinin, and *Phaseolus vulgaris* leukoagglutinin) (Kitagaki-Ogawa *et al.*, 1990). In addition, the *N*-linked oligosaccharide structures of porcine (Yoneda *et al.*, 1993) and human plasma vitronectins (Ogawa *et al.*, 1995) have been elucidated. Carbohydrate composition and lectin reactivity indicate that *N*-glycosylation and sialylation of vitronectin change markedly after partial hepatectomy. Vitronectins from partially hepatectomized rats 24 h after surgery exhibit markedly enhanced binding to Type-I collagen, and equal enhancement of collagen binding was caused by desialylation of vitronectin with sialidase treatment (Uchibori-Iwaki *et al.*, 2000). These results suggest that modulation of the biologic activity of vitronectin is achieved through altered glycosylation. In this study, we demonstrated that vitronectin was modified by diSia. In particular, the amounts of disialylation of vitronectin derived from hepatectomized rat dramatically decreased compared with that of normal rat (Figure 6e), suggesting that diSia residues regulate the function of vitronectin in sera to regenerate the liver. The fact that diSia in sham-operated rat vitronectin decreased compared to that of normal rat suggests that the inflammation caused by tissue injury reduces the disialylation state of vitronectin, although inflammation caused by turpentine oil, which produces the interleukin-1 and interleukin-6 cascade (Won *et al.*, 1993), does not change the disialylation state in serum.

Based on the fact that diSia is present in plasminogen, vitronectin, and α_2 macroglobulin (Kitajima *et al.*, 1999), it might have an important role in the regulation of protease activity. It is noteworthy that some proteases have a basic cluster and a key basic amino acid near active sites that regulates protease activity (Cheng *et al.*, 1986; Rezaie and Yang, 2003). Owing to the negative charge of diSia, it might bind to these basic amino acids to inhibit function. As plasminogen and vitronectin have major roles in fibrinolytic activity in

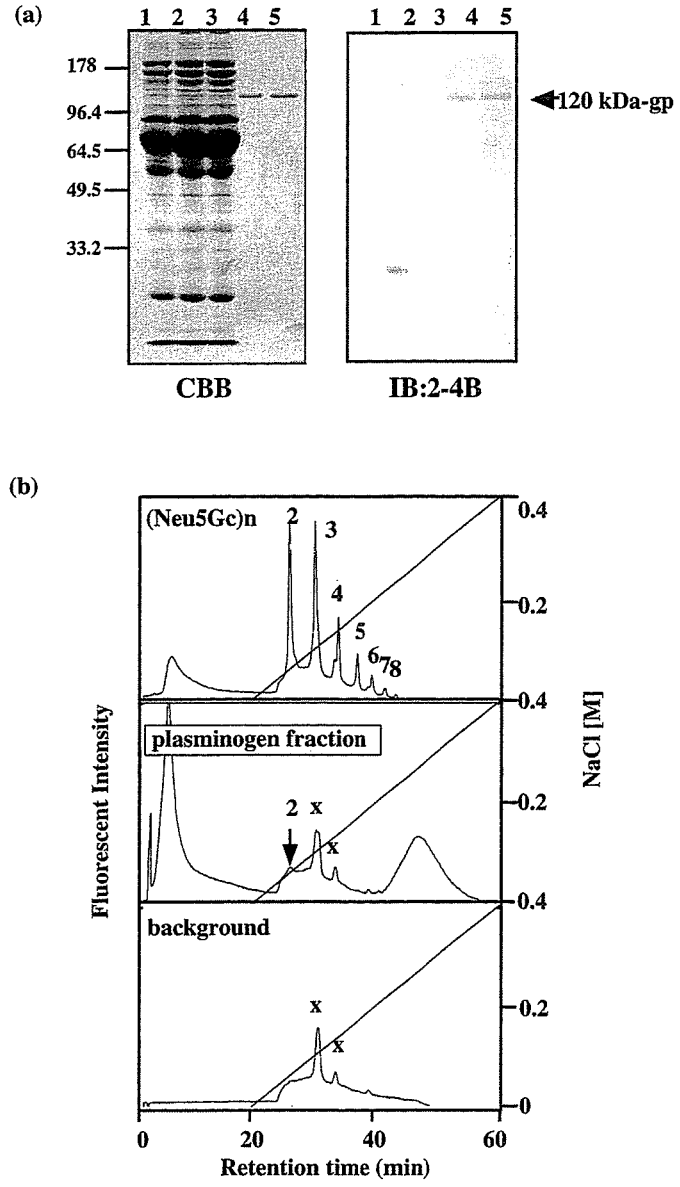

Fig. 5. Affinity-purified plasminogen contained diNeu5Gc residues. (**a**) SDS–PAGE/CBB and western blotting using mAb.2-4B (IB: 2-4B) of the fractions eluted from the lysine-Sepharose. Mouse serum were applied to a lysine-Sepharose and eluted as described in *Materials and Methods*. Mouse serum (15 μg, lane 1), flow-through from non-coupled Sepharose 4B (15 μg, lane 2), flow-through from lysine-Sepharose (15 μg, lane 3), 300 mM phosphate buffer (pH 7.4) eluate (0.2 μg, lane 4), and 0.1 M 6-aminohexanoic acid in 100 mM phosphate buffer (pH 7.4) eluate (0.2 μg, lane 5) were analyzed. Positions of the molecular mass markers are indicated on the left. (**b**) Resource Q anion-exchange chromatography of di/oligo/polyNeu5Gc–DMB. *Upper panel*: α2→8-linked di/oligo/polyNeu5Gc derived from mild acid hydrolysates of polysialoglycoprotein [(Neu5Gc)*n*, 2 μg as Neu5Gc]. The conditions were described in *Materials and Methods* and in Figure 4b. Middle panel: 120-kDa gp of plasminogen fraction (5.4 μg as bovine serum albumin) was treated with 0.01 N trifluoroacetic acid at 50°C for 1 h, and released sialyloligomer was labeled with DMB. Labeled sialyloligomer was applied to the high-performance liquid chromatography analysis as described above. The peak labeled 'x' indicates an unidentified peak that is also detected in background (bottom panel).

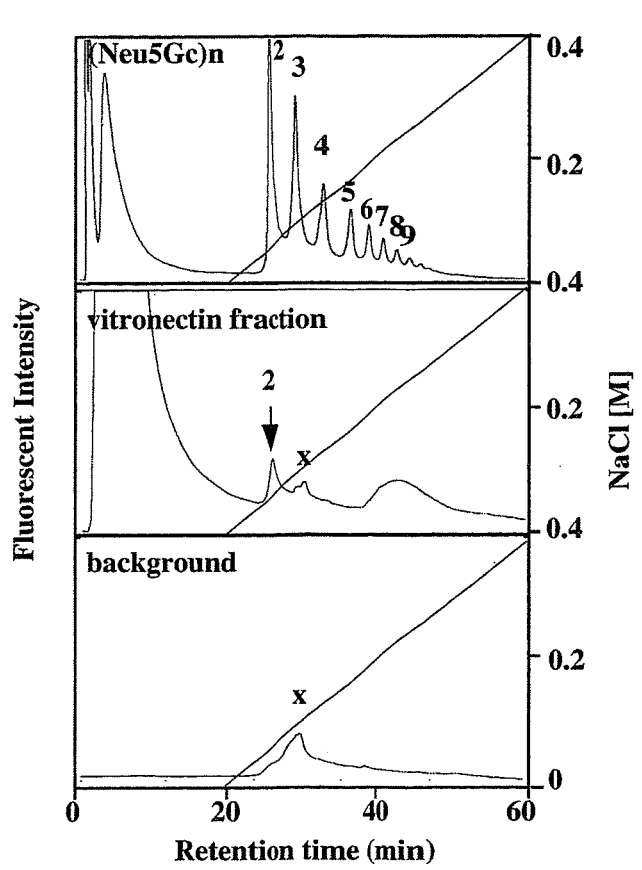

Fig. 6. Mouse and rat vitronectin contained diNeu5Gc and diNeu5Ac, respectively, and the diNeu5Ac residues on rat vitronectin decreased after partial hepatectomy. (**a**) Resource Q anion-exchange chromatography of di/oligo/polyNeu5Gc–DMB. Upper panel: α2→8-linked di/oligo/polyNeu5Gc derived from mild acid hydrolysates of polysialoglycoprotein [(Neu5Gc)*n*, 2 μg as Neu5Gc] labeled with DMB were applied to a Resource Q anion-exchange column (1 mL, Cl^- form). The conditions are described in *Materials and Methods* and in Figure 4b. Middle panel: 70-kDa gp of vitronectin fraction (21 μg as BSA) was treated with 0.01 N trifluoroacetic acid at 50°C for 1 h, and released sialyloligomer was labeled with DMB. Labeled sialyloligomer was applied to a high-performance liquid chromatograph as described above. The peak labeled 'x' indicates an unidentified peak that was also detected in the background (bottom panel). (**b**) SDS–PAGE/silver staining (silver) and western blot analysis using mAb.S2-566 (IB: S2-566 [specific to Neu5Acα2→8Neu5Acα2→3Gal structure]) of vitronectin from normal rat serum. Positions of molecular mass markers are indicated on the left. (**c**) Resource Q anion-exchange chromatography of di/oligo/polyNeu5Ac–DMB. Upper panel: α2→8-linked di/oligo/polyNeu5Ac derived from mild acid hydrolysates of colominic acid [(Neu5Ac)*n*, 10 μg as Neu5Ac] labeled with DMB were applied to a Resource Q anion-exchange column (1 mL, Cl^- form). The conditions are described in the *Materials and Methods* and in Figure 4b. Middle panel: Purified rat vitronectin (3.2 μg as BSA) was treated with 0.01 N trifluoroacetic acid at 50°C for 1 h, and released sialyloligomer was labeled with DMB. Labeled sialyloligomer was applied to the high-performance liquid chromatograph as described above. The peak labeled 'x' indicates an unidentified peak that was also detected in the background (bottom panel). (**d**) SDS–PAGE/silver staining (silver) and western blotting using mAb.S2-566 of vitronectin derived from non-operated rat (NO-VN), sham-operated rat (SH-VN), and partially hepatectomized rat (PH-VN). Vitronectin (0.1 μg/lane) was analyzed. (**e**) The ratio of the amount of diNeu5Ac on vitronectin to the protein amount of vitronectin decreased after partial hepatectomy. The amount of diNeu5Ac and the protein of vitronectin were densitometrically quantified, and the relative ratio of disialic acid to the protein amount of the vitronectin derived from normal serum was set equal to 1.0. The bars indicate standard deviation ($n = 3$).

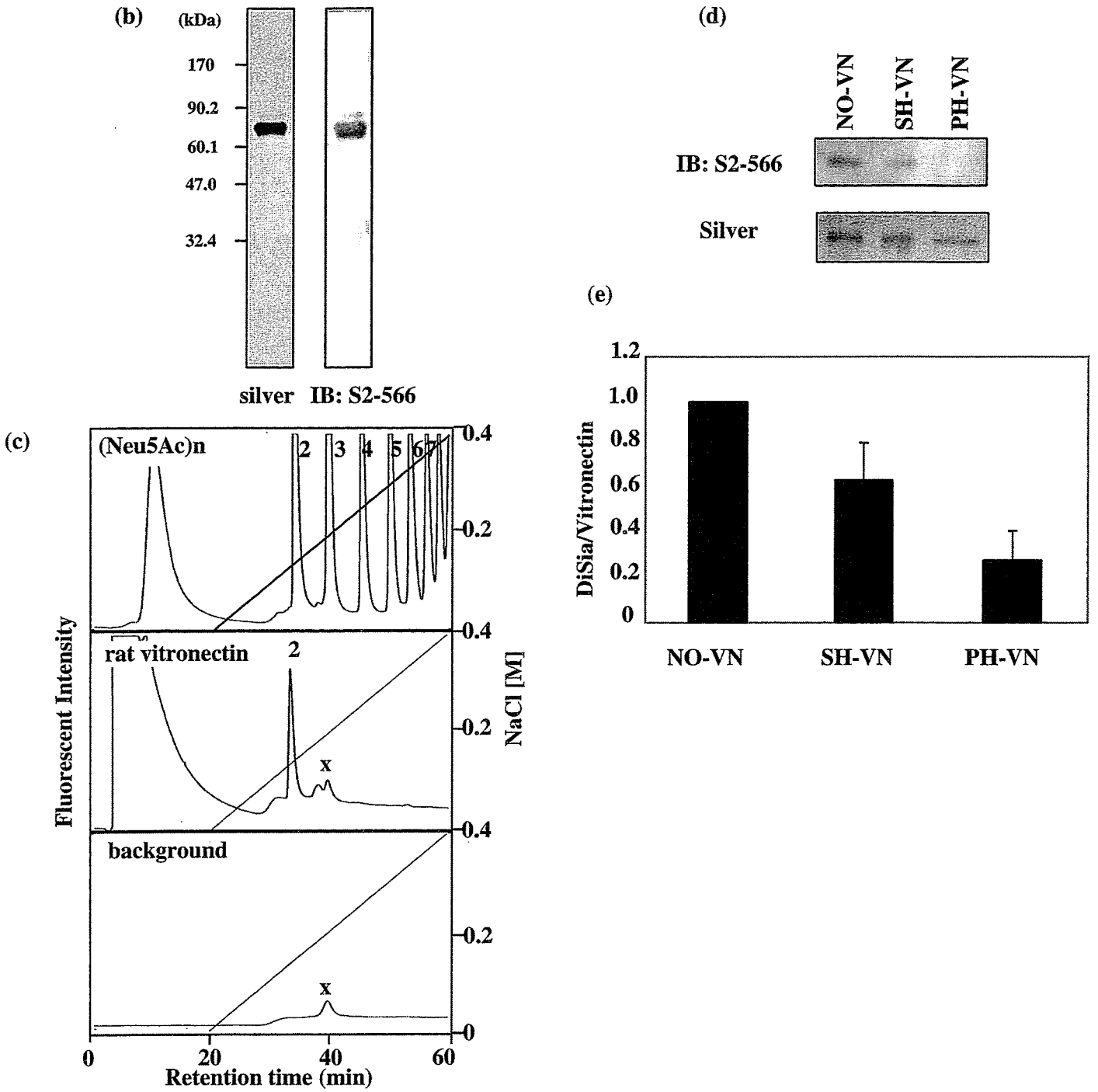

Fig. 6. continued

sera, diSia might regulate fibrinolytic activity via inhibition of proteases in sera.

It has been shown that two sialyltransferases, ST8Sia III and VI, are responsible for the synthesis of diSia structures. ST8Sia III catalyzes the synthesis of disialic and oligosialic acids on glycolipids, glycoproteins, and oligosaccharides (Yoshida *et al.*, 1995; Angata *et al.*, 2000), whereas ST8Sia VI acts on *O*-glycans as well as oligosaccharides (Takashima *et al.*, 2002; Teintenier-Lelievre *et al.*, 2005). ST8Sia III is strongly expressed in fetal brain and testis (Tsuji, 1999). We reported that ST8Sia III was moderately up-regulated during neural differentiation of Neuro2A cells (Sato *et al.*, 2002) and during adipogenesis of 3T3-L1 cells (Sato *et al.*, 2001). The expression of ST8Sia VI is ubiquitous in various cells and tissues (Takashima *et al.*, 2002). In mouse liver, we previously demonstrated that ST8Sia III and VI were constantly expressed before and after inflammation (Yasukawa *et al.*, 2005). Therefore, these sialyltransferases might synthesize the diSia structure on vitronectin, plasminogen, and the light chain of antibodies.

In serum, natural antibodies are present, and sometimes, these antibodies are involved in diseases such as neuropathy (Kornberg and Pestronk, 1995). The antigens of these antibodies are sometimes considered to be gangliosides (O'Hanlon *et al.*, 2002; Schwerer, 2002), which are mimicked by some bacterial lipopolysaccharides or lipooligosaccharides. In this study, we demonstrated the presence of diSia in serum glycoproteins. Thus, diSia might be an immunogen that induces the production of anti-ganglioside antibodies that are sometimes present in sera as natural antibodies.

Materials and Methods

Materials

Silver Stain II Kit Wako was obtained from Wako Pure Chemical (Osaka, Japan). Sephacryl S-100, Protein G-Sepharose, CNBr-activated Sepharose resins, and enhanced chemiluminescence reagents were purchased from Amersham Biosciences (Piscataway, NJ). DEAE-Toyopearl 650 M resins were purchased from Tosoh (Tokyo, Japan). Polyvinylidene difluoride (PVDF) membrane (Immobilon P) was a product obtained from Millipore (Bedford, MA). Prestained molecular weight markers were purchased from Bio-Rad (Hercules, CA), Daiichi Pure Chemicals (Tokyo, Japan), or Sigma Chemical (St. Louis, MO). Peroxidase-conjugated rat anti-mouse IgG was purchased from American Qualex (San Clemente, CA). Peroxidase-conjugated rat anti-mouse IgM was purchased from Zymed Laboratories, (San Francisco, CA). Mouse monoclonal IgM antibody 2-4B, which recognizes Neu5Gcα2→(8Neu5Gcα2→)$_{n-1}$, $n \geq 2$, was prepared as described previously (Sato *et al.*, 1998). DMB was purchased from Dojindo (Kumamoto, Japan). Male, 8-week-old ddY mice were obtained from Japan SLC, (Hamamatsu, Japan). Turpentine oil was kindly provided by Dr. Hiroaki Oda (Nagoya University, Nagoya, Japan). Avidin–biotin–peroxidase complex was obtained from Vectastain ABC Kit (Vector Laboratories, Burlingame, CA). mAbs., mAb.4D4 (IgG1), mAb.5D4 (IgG1), mAb.5E9 (IgG1), mAb.6C6 (IgG1), mAb.L101 (IgG1), mAb.4A1 (IgE), and mAb.9E4 (IgE) were kindly provided by Dr. Tsukasa Matsuda (Nagoya University). mAb.AC1 (IgG3), mAb.9E10 (IgG1) and mAb.735 (IgG2a), and mAb.S2-566 (IgM) were kindly provided by Dr. Keiko Nohara (National Institute of Environmental Studies, Tsukuba, Japan), Dr. Rita Gerady-Schahn (Medizinische Hochschule, Hannover, Germany), and Dr. Koichi Furukawa (Nagoya University), respectively.

Experimental inflammation

Turpentine oil was injected subcutaneously into ddY mice to induce inflammation, and sera were prepared as described previously (Yasukawa *et al.*, 2005).

Purification of the 30- and 120-kDa gp from mouse serum

Normal mouse sera (9.3 mL) was mixed with 9.3 mL of saturated $(NH_4)_2SO_4$ (final concentration, 50%), stirred at 4°C for 1 h and centrifuged at 10,000 × *g* for 10 min. The pellet was dissolved in 10 mM Tris–HCl (pH 8.0) containing 0.1 M NaCl and applied to Sephacryl S-100 chromatography (1.3 × 75 cm, 100 mL, equilibrated with 10 mM Tris–HCl [pH 8.0] containing 0.1 M NaCl). The elution profile was monitored by absorbance at 280 nm and by SDS–PAGE followed by CBB staining. Glycoproteins were separated by SDS–PAGE and electroblotted onto a PVDF membrane and immunostained with mAb.2-4B. The fractions containing mAb.2-4B-immunoreactive 30 and 120-kDa gp were pooled, applied to DEAE-Toyopearl 650 M chromatography (column size: 1.2 × 1.7 cm, buffer: 10 mM Tris–HCl [pH 8.0] containing 10 mM NaCl), and eluted with a linear gradient of 10–70 mM NaCl in 10 mM Tris–HCl (pH 8.0). The elution profile was monitored by the absorbance at 280 nm and by SDS–PAGE followed by CBB staining and western blotting using mAb.2-4B.

Purification of the 70-kDa gp from mouse serum

Inflamed mouse sera (20 mL) was mixed with 20 mL of saturated $(NH_4)_2SO_4$ (final concentration, 50%), stirred at 4°C for 3 h, and centrifuged at 10,000 × *g* for 15 min. The supernatant was mixed with 26.6 mL of saturated $(NH_4)_2SO_4$ (final concentration, 70%), stirred at 4°C for 12 h, and centrifuged at 10,000 × *g* for 15 min. The pellet was dissolved in 50 mM Tris–HCl (pH 8.0) containing 50 mM NaCl and applied to Sephacryl S-100 chromatography (1.3 × 80.5 cm, equilibrated with 50 mM Tris–HCl [pH 8.0] containing 50 mM NaCl). Elution was monitored as described *Purification of the 30-and 120-kDa mouse serum*. The fractions containing the 70-kDa gp were pooled, applied to DEAE-Toyopearl 650 M chromatography (column size: 1.0 × 24 cm, buffer: 50 mM Tris–HCl [pH 8.0] containing 50 mM NaCl), and eluted in a step-wise manner with 0.05, 0.1, 0.15, 0.3, and 1.0 M NaCl containing 50 mM Tris–HCl (pH 8.0). The 70-kDa gp was purified in the 1.0 M NaCl-eluted fraction.

SDS–PAGE and western blotting

Samples were dissolved in Laemmli buffer with 5% mercaptoethanol and boiled at 100°C for 3 min. The samples were electrophoresed in 7 or 10% polyacrylamide gels and visualized by CBB or silver staining. Glycoproteins were electroblotted onto PVDF membranes using a semidry blotting apparatus. The membrane was blocked with 10 mM sodium phosphate buffer (pH 7.2) and 0.15 M NaCl with 0.05% Tween-20 containing 1% bovine serum albumin at 25°C for 1 h. The membrane was incubated with a primary antibody, mAb.2-4B (0.50 μg/mL) or mAb.S2-566 (1.0 μg/mL) at 4°C for 16 h. The secondary antibody was peroxidase-conjugated anti-mouse IgM (1/5000 diluted). Color development was performed as described earlier (Sato *et al.*, 2000).

Two-dimensional gel electrophoresis

Two-dimensional PAGE was performed with a PROTEAN IEF Cell (Bio-Rad) using 7-cm pH 3–10 ReadyStrip IPG Strip (Bio-Rad). Protein samples were resuspended in rehydration buffer (9.8 M urea, 4% CHAPS, and 100 mM dithiothreitol [DTT]) at a ratio of 1 : 3. Isoelectric focusing was performed at 250 V for 15 min, 250–4000 V linear ramp for 2 h, and 4000 V for 5 h at 20°C. After the gel strips were equilibrated for 10 min in 6 M urea, 2% SDS, 0.375 M Tris–HCl (pH 8.8), 20% glycerol, and 130 mM DTT, and then re-equilibrated for 10 min in the same buffer containing 135 mM iodoacetamide in place of DTT. The proteins were separated by SDS–PAGE.